Ore Geology Reviews 63 (2014) 209–225

Contents lists available at ScienceDirect

Ore Geology Reviews

journal homepage: www.elsevier.com/locate/oregeorev

Geology, isotope geochemistry and ore genesis of the Shanshulin carbonate-hosted Pb–Zn deposit, southwest China

Jia-Xi Zhou [a,b,c,*], Zhi-Long Huang [a], Zhi-Cheng Lv [b], Xiang-Kun Zhu [c,**], Jian-Guo Gao [d], Hassan Mirnejad [e]

[a] State Key Laboratory of Ore Deposit Geochemistry, Institute of Geochemistry, Chinese Academy of Sciences, Guiyang 550002, China
[b] Development and Research Center, China Geological Survey, Beijing 100037, China
[c] Laboratory of Isotope Geology, Ministry of Land and Resources, State Key Laboratory of Continental Dynamics, Institute of Geology, Chinese Academy of Geological Sciences, Beijing 100037, China
[d] Faculty of Land Resource and Engineering, Kunming University of Science and Technology, Kunming 650093, China
[e] Department of Geology, Faculty of Sciences, University of Tehran, Tehran 14155-64155, Iran

ARTICLE INFO

Article history:
Received 29 December 2013
Received in revised form 4 May 2014
Accepted 6 May 2014
Available online 20 May 2014

Keywords:
C–O–S–Zn–Pb–Sr isotopes
Sources of ore-forming fluids and metals
Variations of Zn isotope values
Fractional crystallization
Shanshulin Pb–Zn deposit
Southwest China

ABSTRACT

The Shanshulin Pb–Zn deposit occurs in Upper Carboniferous Huanglong Formation dolomitic limestone and dolostone, and is located in the western Yangtze Block, about 270 km west of Guiyang city in southwest China. Ore bodies occur along high angle thrust faults affiliated to the Weishui regional fault zone and within the northwestern part of the Guanyinshan anticline. Sulfide ores are composed of sphalerite, pyrite, and galena that are accompanied by calcite and subordinate dolomite. Twenty-two ore bodies have been found in the Shanshulin deposit area, with a combined 2.7 million tonnes of sulfide ores grading 0.54 to 8.94 wt.% Pb and 1.09 to 26.64 wt.% Zn. Calcite samples have $\delta^{13}C_{PDB}$ and $\delta^{18}O_{SMOW}$ values ranging from −3.1 to +2.5‰ and +18.8 to +26.5‰, respectively. These values are higher than mantle and sedimentary organic matter, but are similar to marine carbonate rocks in a $\delta^{13}C_{PDB}$ vs. $\delta^{18}O_{SMOW}$ diagram, suggesting that carbon in the hydrothermal fluid was most likely derived from the carbonate country rocks. The $\delta^{34}S_{CDT}$ values of sphalerite and galena samples range from +18.9 to +20.3‰ and +15.6 to +17.1‰, respectively. These values suggest that evaporites are the most probable source of sulfur. The $\delta^{34}S_{CDT}$ values of symbiotic sphalerite–galena mineral pairs indicate that deposition of sulfides took place under chemical equilibrium conditions. Calculated temperatures of S isotope thermodynamic equilibrium fractionation based on sphalerite–galena mineral pairs range from 135 to 292 °C, consistent with previous fluid inclusion studies. Temperatures above 100 °C preclude derivation of sulfur through bacterial sulfate reduction (BSR) and suggest that reduced sulfur in the hydrothermal fluid was most likely supplied through thermo-chemical sulfate reduction (TSR). Twelve sphalerite samples have $\delta^{66}Zn$ values ranging from 0.00 to +0.55‰ (mean +0.25‰) relative to the JMC 3-0749L zinc isotope standard. Stages I to III sphalerite samples have $\delta^{66}Zn$ values ranging from 0.00 to +0.07‰, +0.12 to +0.23‰, and +0.29 to +0.55‰, respectively, showing the relatively heavier Zn isotopic compositions in later versus earlier sphalerite. The variations of Zn isotope values are likely due to kinetic Raleigh fractional crystallization. The $^{206}Pb/^{204}Pb$, $^{207}Pb/^{204}Pb$ and $^{208}Pb/^{204}Pb$ ratios of the sulfide samples fall in the range of 18.362 to 18.573, 15.505 to 15.769 and 38.302 to 39.223, respectively. The Pb isotopic ratios of the studied deposit plot in the field that covers the upper crust, orogenic belt and mantle Pb evolution curves and overlaps with the age-corrected Proterozoic folded basement rocks, Devonian to Lower Permian sedimentary rocks and Middle Permian Emeishan flood basalts in a $^{207}Pb/^{204}Pb$ vs. $^{206}Pb/^{204}Pb$ diagram. This observation points to the derivation of Pb metal from mixed sources. Sphalerite samples have $^{87}Sr/^{86}Sr_{200\ Ma}$ ratios ranging from 0.7107 to 0.7115 similar to the age-corrected Devonian to Lower Permian sedimentary rocks (0.7073 to 0.7111), higher than the age-corrected Middle Permian basalts (0.7039 to 0.7078), and lower than the age-corrected Proterozoic folded basement (0.7243 to 0.7288). Therefore, the Sr isotope data support a mixed source. Studies on the geology and isotope geochemistry suggest that the Shanshulin deposit is a carbonate-hosted, thrust fault-controlled, strata-bound, epigenetic, high grade deposit formed by fluids and metals of mixed origin.

1. Introduction

Sediment-hosted Pb–Zn deposits, of which the carbonate-hosted Pb–Zn deposit is an important subtype, are widely represented around the world (Leach et al., 2005, 2010). The best known deposits occur in the mid-continent region of the United States (e.g. Sverjensky, 1981),

* Correspondence to: J.-X. Zhou, State Key Laboratory of Ore Deposit Geochemistry, Chinese Academy of Sciences, Guiyang 550002, China. Tel.: +86 851 5895900; fax: +86 851 5891664.
** Corresponding author.
E-mail addresses: zhoujiaxi@vip.gyig.ac.cn (J.-X. Zhou), xiangkun@cags.ac.cn (X.-K. Zhu).

http://dx.doi.org/10.1016/j.oregeorev.2014.05.012
0169-1368/

Pine Point, Canada (e.g. Powell and Macqueen, 1984), Silesia, Europe (e.g. Heijlen et al., 2003), and Sichuan–Yunnan–Guizhou (SYG) provinces, China (e.g. Pirajno, 2013; Zaw et al., 2007; Zhou et al., 2013a). The SYG Pb–Zn metallogenic province has large deposits of Pb and Zn, among which are the world-class deposits of Huize, Maoping and Daliangzi (e.g. Cromie et al., 1996; Han et al., 2007a, 2007b; Zheng and Wang, 1991; Zhou et al., 2001). The district contains total Pb and Zn metal reserves of more than 20 million tonnes (Mt) at average grades of 5 wt.% Pb and 10 wt.% Zn (Zhou et al., 2013b), and is the major source of base metals in China (Liu and Lin, 1999). Due to the lack of constraints on the origin of these deposits, despite some recently published studies (Han et al., 2007a; Hu and Zhou, 2012; Huang et al., 2010; Li et al., 2007a, 2007b; Ye et al., 2011; Zhou et al., 2013c, 2013d, 2014), there are still many unknown aspects regarding the source of hydrothermal fluids, ore genesis, and geodynamic setting of the Pb–Zn deposits in the SYG province. The Shanshulin Pb–Zn deposit, hosted by dolomitic limestone and dolostone of the Upper Carboniferous Huanglong Formation, is located in the western Yangtze Block, about 270 km west of Guiyang city in southwest China (Fig. 1A). It is the largest Pb–Zn deposit in the southeastern part of the SYG metallogenic province. It has been mined since 1958 and is still in production.

Isotope geochemistry is a powerful tool for determining the source of ore-forming fluids and metals. For example, C, O and S isotopes have been widely used to constrain the origin of hydrothermal fluids (e.g. Basuki et al., 2008; Demény and Harangi, 1996; Dixon and Davidson, 1996; Ohmoto and Goldhaber, 1997; Zhou et al., 2013e),

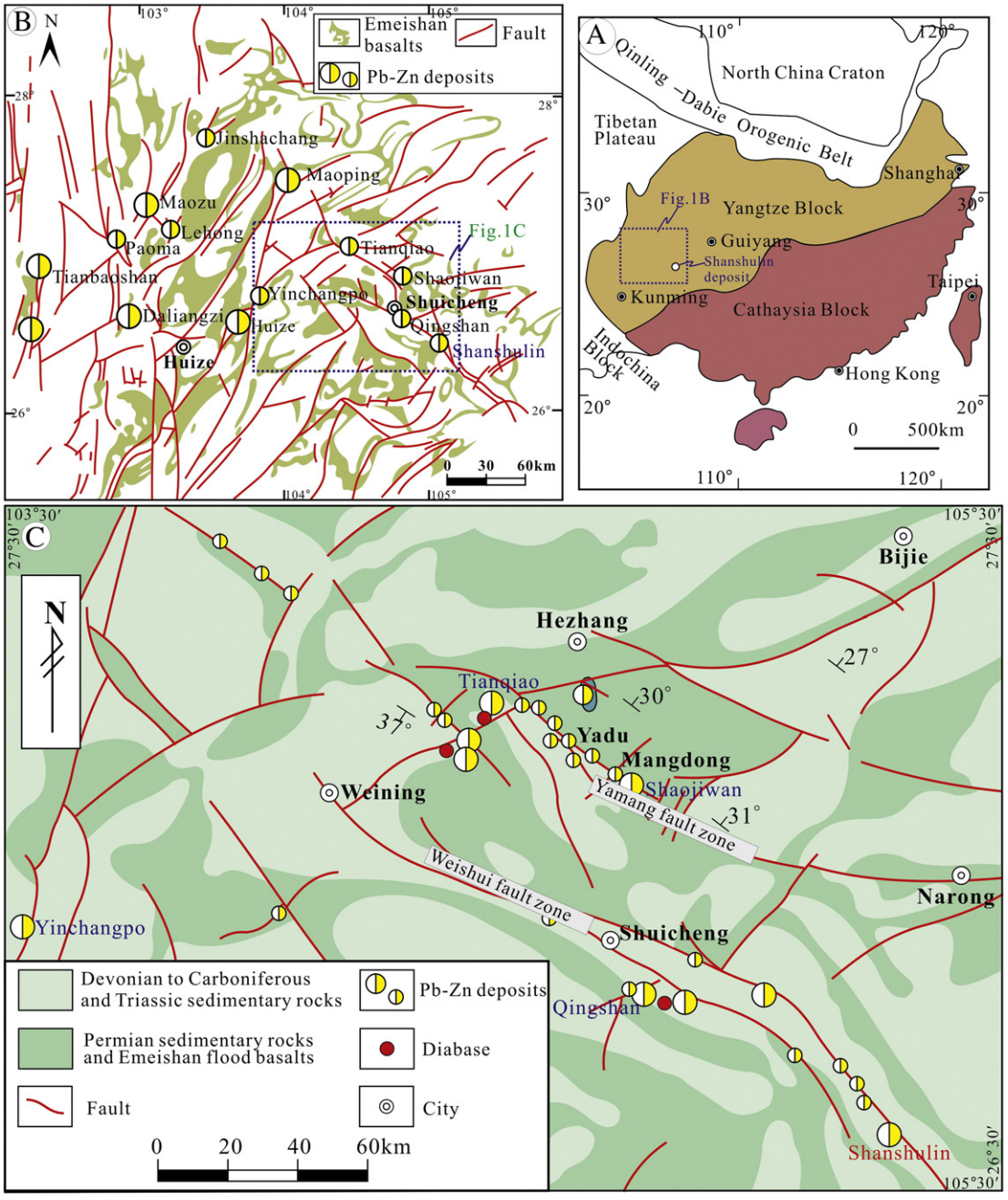

Fig. 1. A: Regional map showing the tectonic setting of the Sichuan–Yunnan–Guizhou (SYG) Pb–Zn metallogenic province; B: simplified map of the SYG province showing faults, Emeishan basalts and typical Pb–Zn deposits; C: geological map of the southeast SYG province showing lithologies, structures and distribution of Pb–Zn deposits.

and Pb and Sr isotopes are useful for tracing the source of ore-forming metals (e.g. Carr et al., 1995; Deng et al., 2000; Fontbote and Gorzawski, 1990; Gromek et al., 2012; Mirnejad et al., 2011; Zhou et al., 2001). In addition, the Zn isotopes have recently been used as a potential tool for understanding the geochemical processes of zinc extraction, transportation and deposition in hydrothermal systems (e.g. Chen et al., 2013; Fujii et al., 2011; Gagnevin et al., 2012; John et al., 2008; Kelley et al., 2009; Mason et al., 2005; Toutain et al., 2008; Wilkinson et al., 2005; Zhou et al., 2014). In this paper, we describe the geology of the Shanshulin Pb–Zn deposit in detail and report new C and O isotopic data of calcite, the first Zn and Sr isotopic data of sulfide minerals and sedimentary country rocks, and additional S and Pb isotopic data of sulfide minerals. This new dataset, together with the previously published results, are used to understand the source of ore-forming fluids and metals, the possible genesis of the Pb–Zn ores, and the ore-forming geodynamic setting of the Shanshulin deposit. These results are also used to discuss the possible controls on variations of Zn isotope values during Pb–Zn mineralization and the causes of highly concentrated base metals in the SYG province.

2. Geological setting

2.1. Regional geology

South China is made up of the Yangtze Block to the north and the Cathaysian Block to the south (Fig. 1A). The Archean crystalline basement (Gao et al., 2011; Qiu et al., 2000), Meso- to Neoproterozoic folded basement (Wang et al., 2012; Zhao et al., 2010) and Paleozoic to Mesozoic cover sequence (Fu, 2004; Liu and Lin, 1999) constitute the Yangtze Block. In the western part of the Yangtze Block, the folded basement includes the ~1.7 Ga Dongchuan and ~1.1 Ga Kunyang/Huili Groups and equivalents (Sun et al., 2009; Wang et al., 2010) that consist of greywacke, slate and other carbonaceous and siliceous sedimentary rocks. These rocks are unconformably overlain by shallow marine Paleozoic and Early Mesozoic cover sequence (Liu and Lin, 1999; Yan et al., 2003). Evaporites are common in Cambrian to Triassic sedimentary rocks (Zhou et al., 2013a). Late Mesozoic (Cretaceous) to Cenozoic lithologies are composed entirely of a continental sequence (Liu and Lin, 1999). A major feature of the western Yangtze Block is the Middle–Late Permian (267–256 Ma) Emeishan Large Igneous Province and its flood basalts that cover an area of more than 250,000 km^2 (Jian et al., 2009; Zhou et al., 2002). After eruption of the Emeishan basalts, the western Yangtze Block collided with the adjacent Yidun arc resulting in closure of the Tethys Ocean (e.g. Reid et al., 2007; Zhou et al., 2013a, 2013d). This event is known as the Indosinian Orogeny (257–205 Ma) and it resulted in deformation of the rocks by thrust faults and folds (e.g. Han et al., 2007a; Hu and Zhou, 2012; Zhou et al., 2013a). Tectonics, magma and ore deposits formed in the Indosinian in the Yangtze Block have been affected by the later Yanshanian (205–65 Ma) and Himalayan (65–0 Ma) orogenic events (e.g. Liu and Lin, 1999; Zaw et al., 2007).

More than 400 Pb–Zn deposits have been reported in the SYG province, which are distributed in a large triangular area of 170,000 km^2 (Fig. 1A and B) in NE Yunnan, NW Guizhou and SW Sichuan provinces (e.g. Han et al., 2007b; Liu and Lin, 1999; Zhou et al., 2013a). Among these deposits, the Huize world-class Zn–Pb–Ge deposit (Fig. 1B) contains more than 5 Mt Pb–Zn metal reserves (Han et al., 2007a; Huang et al., 2003). These deposits in the SYG province are hosted in Neoproterozoic to Lower Permian carbonate rocks that are all overlain by Middle Permian Emeishan flood basalts (e.g. Liu and Lin, 1999; Zheng and Wang, 1991; Zhou et al., 2013b, 2014). Faults in the eastern part of the SYG province trend NW (Fig. 1B; Zhou et al., 2013c), whereas NS- and NE-trending faults are dominant in the western part (Han et al., 2007a; Zhou et al., 2013d). It is evident that these faults strictly control the distribution of Pb–Zn deposits in the SYG province (Fig. 1B and C; Han et al., 2007a; Liu and Lin, 1999; Zheng and Wang, 1991; Zhou et al., 2013e). Geochronological studies in the SYG province have reported hydrothermal calcite/fluorite Sm–Nd isochron ages of the Huize, Maozu and Jinshachang Pb–Zn deposits at 222 ± 14 Ma (Li et al., 2007b), 196 ± 13 Ma (Zhou et al., 2013d) and 201.1 ± 2.9 Ma (Mao et al., 2012), respectively, and sulfide minerals (sphalerite and/or pyrite) Rb–Sr isochron ages of the Paoma, Tianqiao, Jinshachang and Lehong Pb–Zn deposits at 200.1 ± 4.0 Ma (Lin et al., 2010), 191.9 ± 6.9 Ma (Zhou et al., 2013a), 199.5 ± 4.5 Ma and 200.9 ± 2.3 Ma (Mao et al., 2012), respectively. It is possible that the Pb–Zn mineralization in the SYG province was formed in the Late Indosinian to Early Yanshanian (222–192 Ma).

2.2. Geology of the southeast SYG province

In the southeast SYG province where the Shanshulin deposit is located, the Proterozoic folded basement is not exposed. The cover sequence includes Devonian to Triassic sedimentary rocks and Middle Permian Emeishan flood basalts (Fig. 1C). The Devonian strata consist of sandstone, siltstone, limestone and dolostone, and the Carboniferous strata are composed of shale, limestone and dolostone. The Lower Permian sedimentary sequence consists of sandstone, shale, coal and limestone, all of which are overlain by Middle Permian Emeishan flood basalts. The basalts are overlain by Upper Permian sandstone, siltstone and coal strata. The Triassic strata are composed of siltstone, sandstone, dolostone and limestone. Barite and/or gypsum-bearing evaporites are distributed in Devonian to Triassic sedimentary rocks (Jin, 2008; Zhou et al., 2013a). More than 100 Pb–Zn deposits are hosted in Devonian to Lower Permian carbonate rocks (e.g. Jin, 2008; Mao et al., 1998; Zhou et al., 2013b) and occur along the EW-, NE- and NW-trending faults, particularly the NW-trending Weishui (Weining–Shuicheng) and Yamang (Yadu–Mangdong) fault zones (Fig. 1C). The Shanshulin Pb–Zn deposit is located in the southeastern part of the Weishui fault zone and within its thrust faults and fold structures (Figs. 1C and 2).

3. Geology of the Shanshulin deposit

3.1. Stratigraphy and lithology

In the Shanshulin deposit area, the exposed strata include Carboniferous, Permian and Lower to Middle Triassic rocks (Fig. 2). The Carboniferous strata include Lower Carboniferous Dapu and Baizuo Formations, and Upper Carboniferous Huanglong and Maping Formations, all of which mainly consist of limestone, dolomitic limestone and dolostone with minor claystone. The Pb–Zn ore bodies of the Shanshulin deposit are hosted by the dolomitic limestone and dolostone of the Upper Carboniferous Huanglong Formation (Fig. 3). Overlying Carboniferous rocks are shale and coal of the Lower Permian Liangshan Formation and limestone of the Lower Permian Qixia Formation, all of which are overlain by the Emeishan basalts. The basalts are overlain by shale and coal of the Upper Permian Longtan Formation. The Lower to Middle Triassic strata are composed of sandstone, shale, mudstone, and marlstone. Organic matter is widely distributed in the Upper Permian and Lower to Middle Triassic shale and coal.

3.2. Tectonics

There are three main faults and two folds in the Shanshulin deposit area (Fig. 2). The NW-trending Weishui fault zone consists of many high angle thrust faults (such as F_1) with dip angles between 50° and 80°, of which the thrust faults (such as F_9) in the Shanshulin deposit area have dip angles between 55° and 75° (Fig. 3). Pb–Zn ore bodies in the Shanshulin deposit occur along these thrust faults (Fig. 3). The other two faults (F_3 and F_5) are normal (Fig. 2). The Carboniferous and Permian strata form the Guanyinshan anticline, and the Permian and Triassic strata form the Guanyinshan syncline (Fig. 2).

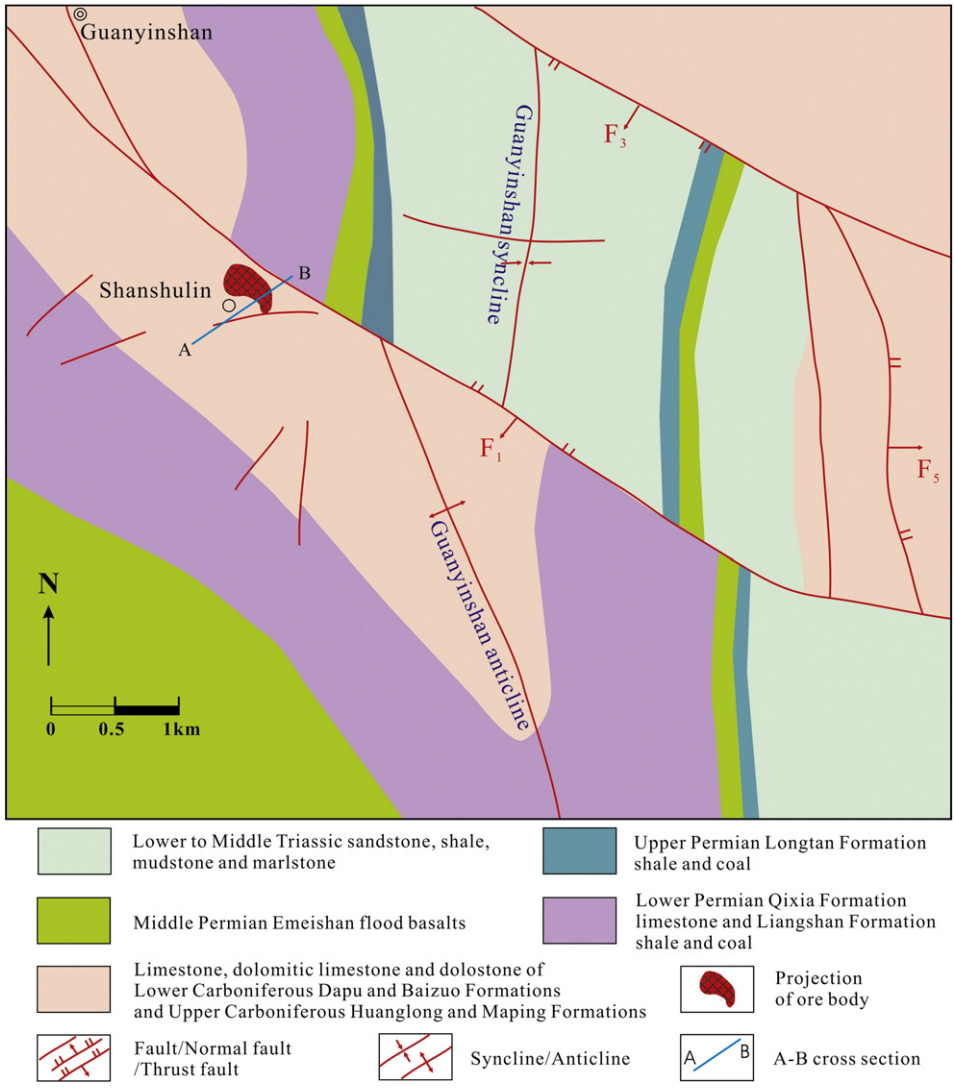

Fig. 2. Geological map of the Shanshulin Pb–Zn deposit showing the lithologies, faults, folds and projection of ore body.

Ore bodies occur within the northwestern part of the Guanyinshan anticline (Fig. 2).

3.3. Ore bodies

The ore bodies in the Shanshulin deposit can be divided into two types: the dominant strata-bound type and the steeply dipping vein type. Twenty-two ore bodies have been found in the Shanshulin deposit area, of which the No. 4 ore body is the largest. This ore body is strata-bound and occurs along the F_9 thrust fault (Figs. 3 and 4E). The ore body is 460 m in length, 200 m in depth, and the mean thickness is 5.2 m. It contains at least 2 Mt sulfide ores at grades of 0.24 to 7.94 wt.% Pb (average 3.64 wt.%) and 1.09 to 26.64 wt.% Zn (average 14.98 wt.%). The steeply dipping veins (include veinlets: Fig. 4B and C and tiny veins: Fig. 4E and F) commonly occur in the upper or lower part of strata-bound ore bodies and contain less than 0.2 Mt sulfide ores grading 0.13 to 3.45 wt.% Pb (average 2.16 wt.%) and 0.85 to 5.65 wt.% Zn (average 3.52 wt.%).

3.4. Texture and structure of the ores

Ores in the Shanshulin deposit underwent hydrothermal and supergene oxidizing processes. Therefore, there are oxidized and sulfide ores along with a mixture of these two types. Sulfide ores are composed of sphalerite, pyrite and galena, accompanied by calcite and dolomite. Oxidized and mixed ores have extremely complex assemblages of smithsonite, limonite, cerusite, sphalerite, pyrite, galena, and carbonate minerals.

Within the sulfide ore zones, structures consist of massive, vein and disseminated types (Figs. 4 and 5), and textures consist of anhedral to euhedral granular (Fig. 6A), filling (Fig. 6B, C and F), and pressure shadows (Fig. 6D and E). In massive ores (Figs. 4A, B, C, 5A and E), brown sphalerite is fine- to coarse-grained (0.1–6 mm) with anhedral to euhedral texture (Fig. 6A, C and F). Pyrite is fine-grained (0.05–0.5 mm), and has cubic form (Fig. 6A, B and C). Calcite occurs as patches that are about 2 cm in width (Figs. 4C, 5D and F). In vein ores, sphalerite is also fine- to coarse-grained (0.05–4 mm) with anhedral to euhedral texture (Figs. 4F and 5F), and is brown and/or brown–yellow in color (Fig. 6F). Associated pyrite is fine-grained (0.01–0.05 mm), and has anhedral form (Fig. 6F). Galena fills tiny vein and fracture (Fig. 6B and C) with individual grains size less than 0.005 mm. Calcite occurs in tiny veins (Fig. 6F). In metasomatic and/or disseminated ores, sphalerite is dominantly brown–yellow in color and fine- to coarse-grained (0.01–3 mm) with anhedral texture (Figs. 4B and 5D). Pyrite metasomatic replacement of sphalerite (Fig. 6F) and galena is disseminated in the previously-formed granular sphalerite (Fig. 4C). Calcite occurs in

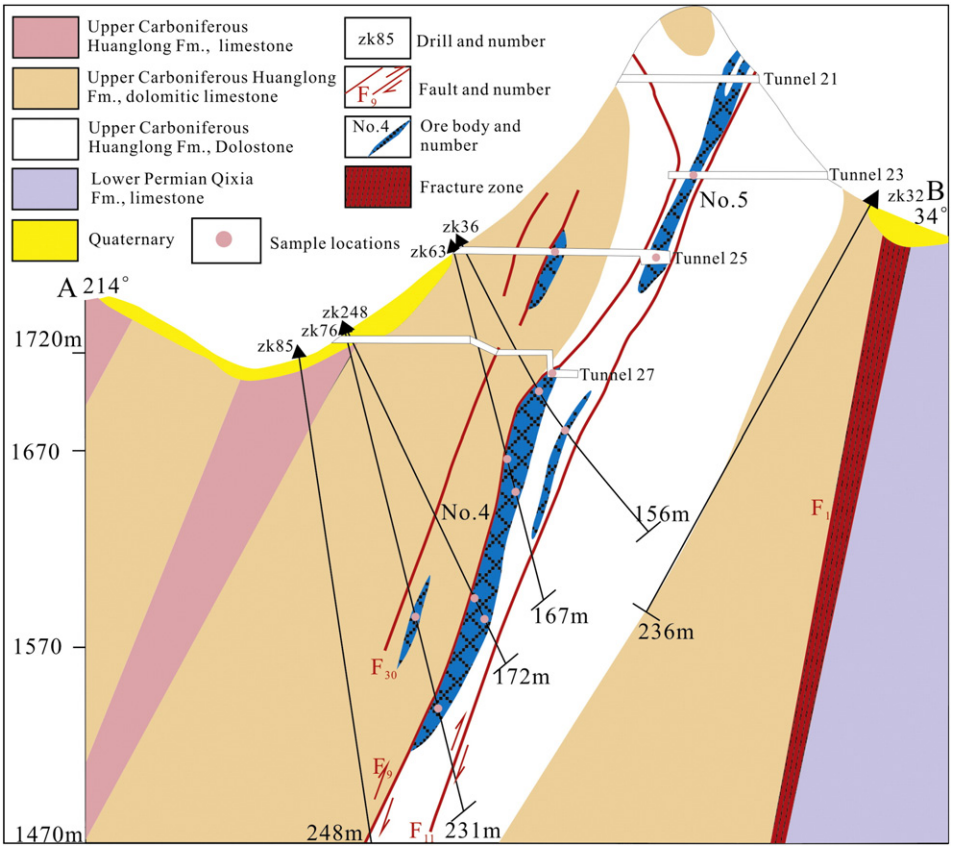

Fig. 3. A–B cross-section of the Shanshulin Pb–Zn deposit showing the drill holes, tunnel locations, ore bodies, ore-controlling thrust faults and host rock lithologies.

spotted granular aggregates (Fig. 5D). In the gangue assemblage, calcite and dolomite (Fig. 4D and F) occur in veinlets and/or tiny veins in dolostone, dolomitic limestone and limestone.

3.5. Mineral paragenesis

Based on crosscutting, overgrowth and replacement relationships, the hydrothermal period is divided into four stages: (I) pyrite + sphalerite + calcite, (II) sphalerite + pyrite + galena + calcite, (III) sphalerite + galena + calcite, and (IV) calcite + dolomite. Stage I sphalerite is brown color and occurs as patches (Fig. 5F). Stage I calcite occurs in anhedral aggregates (Fig. 5F). Stage II sphalerite has a granular shape and brown and/or brown–yellow in color (Figs. 4 and 5), galena occurs in spotted granular aggregates with pressure shadows (Figs. 4C, 5A and 6E) and calcite occurs in 1 to 5 cm veinlets (Fig. 6A and F). Stage III sphalerite is brown–yellow in color (Fig. 6E) and occurs in 1 to 5 cm veinlets (Fig. 4F), galena and calcite occur in 0.5 to 1 cm tiny veins (Figs. 4B, E, F and 5C). Stage IV calcite and dolomite occur in 1 to 5 cm veinlets and 0.5 to 1 cm tiny veins in the host rocks (Fig. 4D). Details about mineral paragenesis are listed in Table 1.

3.6. Wall rock alteration

Wall rock alteration types are simple and include: (i) dolomite, (ii) Fe–Mn carbonates, and (iii) zones of gossan consisting of iron and aluminum oxides and hydroxides. Dolomitization enhances rock brittleness and causes crack opening for Pb–Zn mineralization. Fe–Mn carbonatization forms light brown, maroon and puce Fe/Mn-bearing dolomite and is closely associated with Pb–Zn mineralization. Gossan coexists with Pb–Zn sulfide ores and is usually located in the upper levels of the sulfide ores. The intensity of gossan formation is directly related to Pb–Zn mineralization (Zhou et al., 2013a).

4. Analytical methods

Seventeen representative sulfide ore samples from drill core and mining tunnels were collected (sample locations are shown in Fig. 3). Five brown sphalerite, seven brown–yellow sphalerite, four galena, and nine calcite separates (Tables 3 and 4) were hand picked from these hand specimens using a binocular microscope and analyzed for C, O, S, Zn, Pb and Sr isotopes. In addition, four whole-rock samples of Lower Permian Qixia Formation limestone and Lower Carboniferous Baizuo Formation dolostone were collected for Sr isotopes (Table 8).

4.1. Carbon and oxygen isotope analyses

Carbon and oxygen isotopic compositions were obtained using a Finnigan MAT-253 mass spectrometer at the State Key Lab of Environmental Geochemistry, Chinese Academy of Sciences. Calcite reacted with pure phosphoric acid to produce CO_2. The analytical precision (2σ) is $\pm 0.2‰$ for $\delta^{13}C$ value and $\pm 0.5‰$ for $\delta^{18}O$ value. C and O isotopic compositions are reported relative to the Vienna Pee Dee Belemnite (V-PDB) and Vienna Standard Mean Ocean Water (V-SMOW), respectively.

4.2. Sulfur isotope analysis

Sulfur isotope analysis was undertaken at the State Key Lab of Environmental Geochemistry, Chinese Academy of Sciences, by using continuous flow isotope ratio mass spectrometer. GBW 04415 and GBW 04414 Ag_2S were used as external standards and the Vienna Canyon Diablo Troilite (V-CDT) as reference standard, with an analytical precision of $\pm 0.2‰$ (2σ).

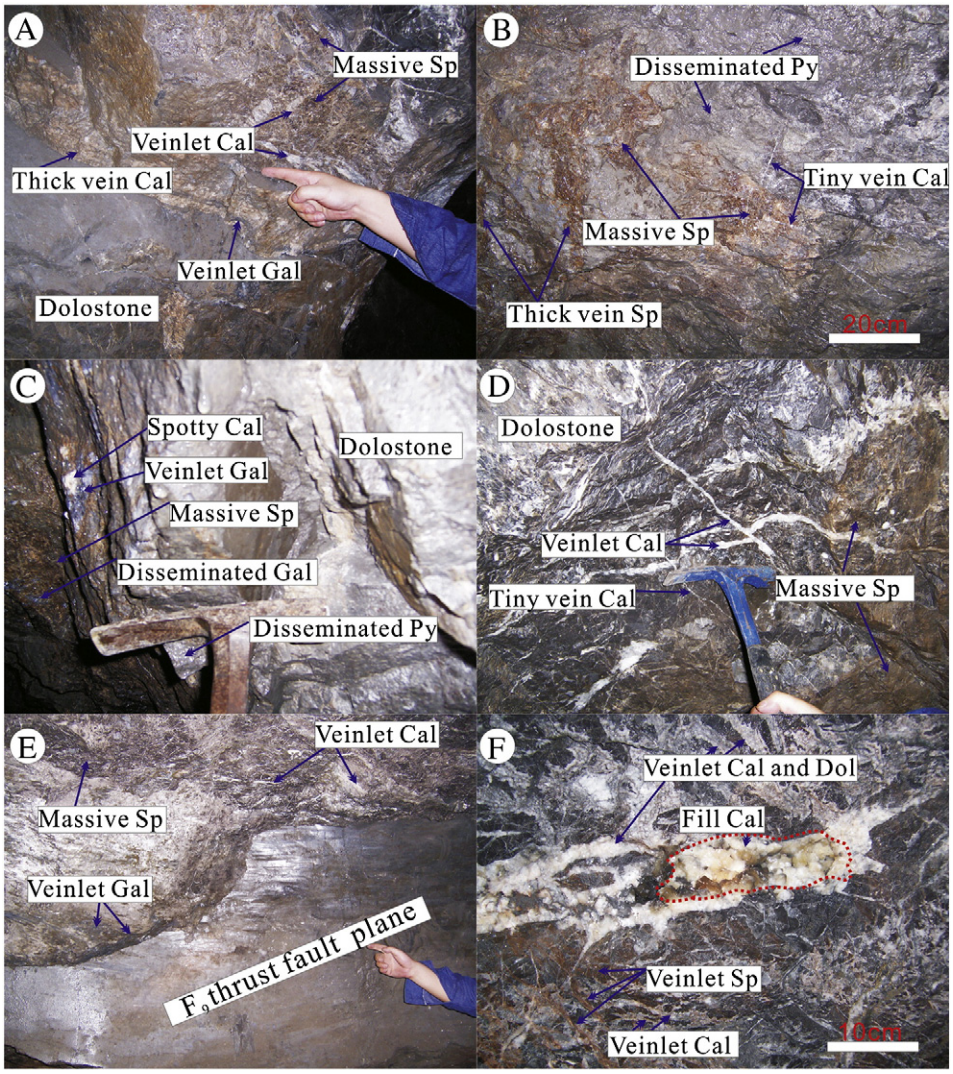

Fig. 4. A: Photograph showing thick vein calcite (Cal) containing veinlet galena (Gal) with veinlet Cal and massive sphalerite (Sp) in dolostone; B: tiny vein Cal within disseminated pyrite (Py) and massive sphalerite (Sp) with thick vein Sp; C: spotty Cal, veinlet Gal and disseminated Gal enclosed in massive Sp and disseminated Py in dolostone; D: veinlet and tiny vein Cal in massive Sp and dolostone; E: veinlet Cal in massive Sp with veinlet Gal in F_9 thrust fault plane; F: fill Cal with veinlet Cal, dolomite (Dol) and Sp in dolostone.

4.3. Zinc isotope analysis

Sphalerite samples were digested in HCl and then taken up in 6N HCl + 0.001% H_2O_2. Zn was separated from matrix elements using anion exchange chromatography (Tang et al., 2006), a modified procedure from that described by Maréchal et al. (1999). H_2O used in the experiment was purified using the Milli-Q system, with electric resistance of 18.2 MΩ. HCl was purified by sub-boiling distillation and the purification of all reagents was completed in an ultraclean laboratory. Zn isotope analysis was carried out using a Nu plasma high resolution multi-collector inductively coupled plasma mass spectrometry (HR MC-ICP-MS) at the Key Laboratory of Isotope Geology, MLR, Institute of Geology, Chinese Academy of Geological Sciences (Li et al., 2008; Zhou et al., 2014). Mass discrimination effects were corrected using a combined sample-standard bracketing and inter-element correction procedure (Li et al., 2008; Mason et al., 2004a, 2004b; Zhu et al., 2000, 2002). Accuracy and reproducibility were assessed by replicate analyses of the international standard BCR-2 (basalt), which yielded an average δ^{66}Zn value of 0.28 ± 0.07 (2σ, n = 6), within errors in agreement with the previously published values by Zhou et al. (2014). Sample SSL1-@1 brown–yellow sphalerite was used for procedural repeat. Each result is the mean value over N number of repeats, and all results are reported relative to the Lyon JMC 3-0749L Zn standard (Maréchal et al., 1999).

4.4. Lead isotope analysis

Lead isotope analysis was carried out using a GV Isoprobe-T thermal ionization mass spectrometer at the Beijing Institute of Uranium Geology. The analytical procedure involved dissolution of samples using HF and $HClO_4$ in crucibles, followed by basic anion exchange resin to purify Pb. Analytical results for the standard NBS 981 are $^{206}Pb/^{204}Pb = 16.937 \pm 0.002$ (2σ, n = 10), $^{207}Pb/^{204}Pb = 15.457 \pm 0.002$ (2σ, n = 10) and $^{208}Pb/^{204}Pb = 36.611 \pm 0.004$ (2σ, n = 10).

4.5. Strontium isotope analysis

Chemical separations of Rb and Sr from matrix elements and mass spectrometric measurements were accomplished at the Institute of Geology and Geophysics, Chinese Academy of Sciences. Spec-Sr exchange resin was used for the separation and purification of Rb and Sr. The procedure blanks of Rb and Sr are about 6 and 5 pg (10^{-12} g), respectively. A detailed analytical procedure for Rb–Sr isotope analysis is available in Li et al. (2005). Rb–Sr isotopic compositions were measured by the GV Isoprobe-T thermal ionization mass spectrometer. An $^{88}Sr/^{86}Sr$ ratio of

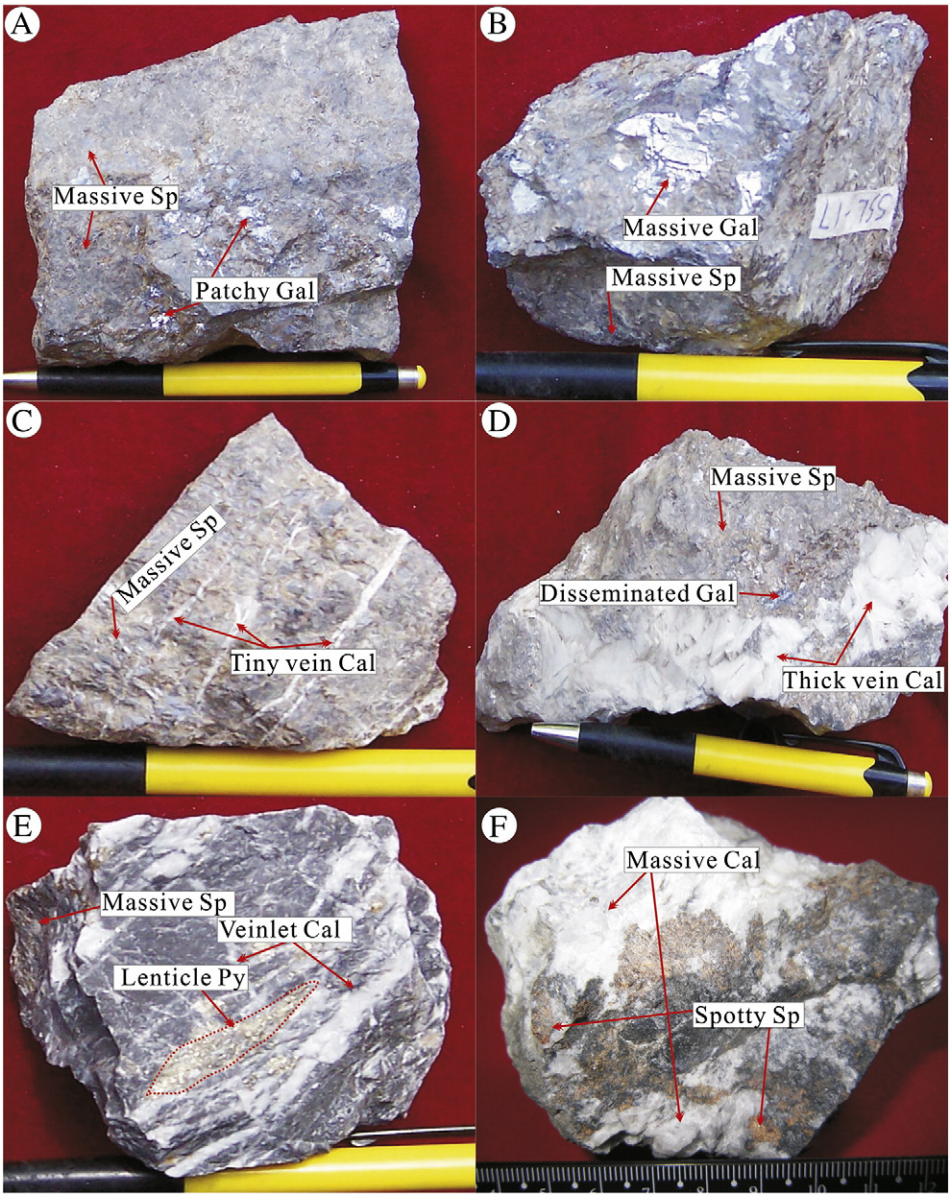

Fig. 5. Ore types of the Shanshulin Pb–Zn deposit. A: Massive ore includes sphalerite (Sp) and patchy galena (Gal); B: massive ore includes Sp and Gal; C: vein ore includes massive Sp and tiny vein calcite (Cal); D: disseminated ore includes massive Sp, disseminated Gal and thick vein Cal; E: vein ore includes massive Sp, veinlet Cal and lenticle Py; F: disseminated ore includes massive Cal and spotty Sp.

8.37521 is used to calibrate mass fractionation of Sr isotope. The average $^{87}Sr/^{86}Sr$ ratio of NBS 987 is 0.710242 ± 5 (2σ, n = 12). The uncertainties (2σ) are 0.005% for $^{87}Sr/^{86}Sr$ ratios and 2% for $^{87}Rb/^{86}Sr$ ratios.

5. Results

5.1. Carbon and oxygen isotopic compositions

C and O isotopic compositions of calcite separates from carbonate host rock and sulfide ore are listed in Table 2 and shown in Fig. 7. Calcite samples have $\delta^{13}C_{PDB}$ and $\delta^{18}O_{SMOW}$ values ranging from −3.1 to +2.5‰ (average −1.0‰, n = 9) and +18.8 to +26.5‰ (average +21.0‰, n = 9), respectively. Stage I calcite samples have $\delta^{13}C_{PDB}$ values ranging from −1.7 to −1.4‰ (average −1.6‰, n = 3) and $\delta^{18}O_{SMOW}$ values ranging from +18.8 to +19.2‰ (average +19.0‰, n = 3). Stage II calcite samples have $\delta^{13}C_{PDB}$ and $\delta^{18}O_{SMOW}$ values ranging from −2.2 to −1.6‰ (average −1.9‰, n = 3) and +19.5 to +20.3‰ (average +19.9‰, n = 3), respectively. The $\delta^{13}C_{PDB}$ and $\delta^{18}O_{SMOW}$ values of Stage III calcite sample are −3.1‰ and +20.2‰, respectively. Stage IV calcite samples have $\delta^{13}C_{PDB}$ values ranging from +2.3 to +2.5‰ (average +2.4‰, n = 2) and $\delta^{18}O_{SMOW}$ values ranging from +25.6 to +26.5‰ (average +26.1‰, n = 2). The $\delta^{13}C_{PDB}$ and $\delta^{18}O_{SMOW}$ values of carbonate whole-rock samples range from −1.8 to +3.9‰ (mean +1.8‰, n = 9) and +21.0 to +26.8‰ (mean +23.2‰, n = 9), respectively (Hu, 1999; Mao et al., 1998). There is no difference in $\delta^{13}C_{PDB}$ and $\delta^{18}O_{SMOW}$ values among Stages I to III calcite samples, but Stage IV calcite samples have $\delta^{13}C_{PDB}$ and $\delta^{18}O_{SMOW}$ values higher than those of Stages I to III calcite and similar to those of the carbonate whole-rock (Fig. 7). It is clear that Stages I to III calcite samples from the Shanshulin deposit have similar $\delta^{13}C_{PDB}$ values but higher $\delta^{18}O_{SMOW}$ values compared with the Huize (Huang et al., 2010) and Tianqiao (Zhou et al., 2013a) deposits, two typical Pb–Zn deposits in the SYG province (Fig. 7).

5.2. Sulfur isotopic compositions

Sulfur isotopic compositions of sulfide samples are given in Table 3 and shown in Fig. 8A and B. The $\delta^{34}S_{CDT}$ values of seven sphalerite

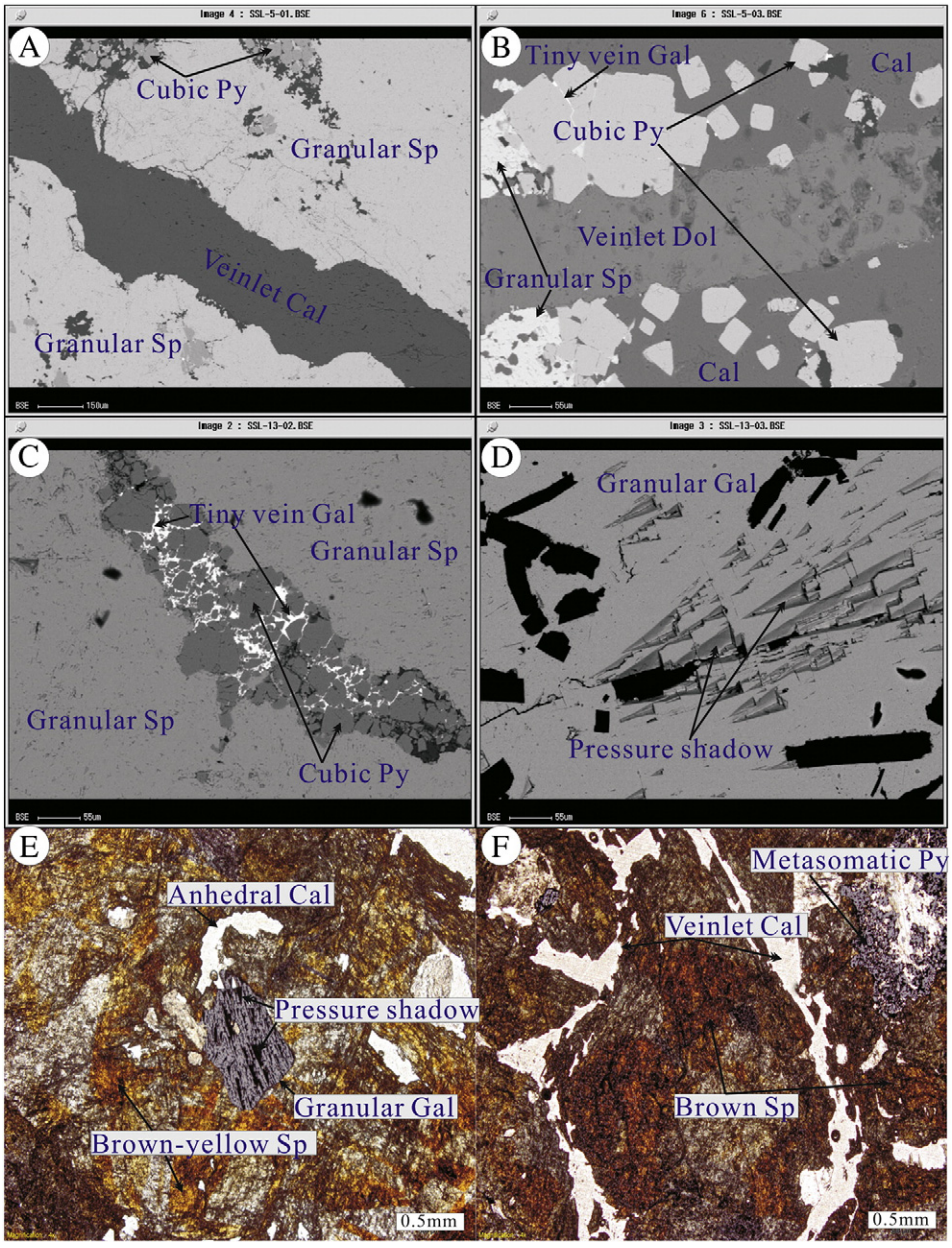

Fig. 6. Electron probe micro-analysis (EPMA) backscattered electron images (A–D) and microscope reflected light photographs (E–F) of sulfide ores from the Shanshulin Pb–Zn deposit. A: cubic pyrite (Py) enclosed in granular sphalerite (Sp) and veinlet calcite (Cal) crosscuts granular Sp; B: tiny vein galena (Gal) filling fracture in cubic Py that intergrown with granular Sp enclosed in Cal and veinlet dolomite (Dol) crosscuts Cal; C: tiny vein Gal filling fractures in cubic Py that enclosed in granular Sp; D: pressure shadow of granular Gal; E: anhedral Cal and pressure shadow of granular Gal enclosed in brown–yellow Sp; F: metasomatic Py and veinlet Cal filling fractures in brown Sp.

Table 1
Mineral paragenesis of the Shanshulin Pb–Zn deposit.

Periods	Hydrothermal				Supergene
Stages	Stage I	Stage II	Stage III	Stage IV	
Mineral assemblages	Sp + Py + Cal	Sp + Py + Gal + Cal	Sp + Gal + Cal	Dol + Cal	Lim + Cer + Smi
Pyrite	▬	▬	—		
Brown Sp	—	▬	—		
Brown–yellow Sp	—	▬	▬		
Galena	—	▬	▬		
Dolomite	—	—	—	▬	
Calcite	▬	▬	▬	▬	
Smithsonite					▬
Limonite					▬
Cerusite					▬

Sp, sphalerite; Py, pyrite; Gal, galena; Dol, dolomite; Cal, calcite; Lim, limonite; Cer, Cerusite.
— Less; ▬ more.

samples from the Shanshulin deposit occupy a narrow range between +18.9‰ and +20.3‰ with an average value of +19.3‰ (Table 3). There is no difference of $\delta^{34}S_{CDT}$ values between Stage II (+19.0 to 20.3‰, average +19.4‰, n = 4) and Stage III (+18.9 to +19.6‰, average +19.2‰, n = 3) sphalerite samples (Fig. 8B). Four galena samples have $\delta^{34}S_{CDT}$ values ranging from +15.6 to +17.1‰ (mean +16.0‰). The $\delta^{34}S_{CDT}$ values of Stage II galena samples (Fig. 8B) range from +15.7 to +15.8‰ (average +15.8‰, n = 2) similar to those of Stage III galena (+15.6 to +17.1‰, average +16.4‰, n = 2). It is obvious that the $\delta^{34}S$ values of sphalerite samples are significantly higher than those of galena (Table 3), especially in the same hand specimens (such as samples SSL6, SSL12 and SSL17; Fig. 8C). The $\delta^{34}S$ values of sphalerite and galena samples in this study are slightly higher than previous reported sulfur isotope data, which range from +15.9 to +18.7‰ and +13.4 to +14.2‰ (Chen, 1986; Fu, 2004), respectively. This may

Table 2
Carbon and oxygen isotopic compositions for the Shanshulin Pb–Zn deposit.

No.	Mineral/rock	Sample types	$\delta^{13}C_{PDB}$/‰	$\delta^{18}O_{SMOW}$/‰	Sources
HTQ-w	Whole-rock	Lower Carboniferous Baizuo Fm., dolostone	−0.8	+23.1	Hu (1999)
HTQ-a	Whole-rock	Lower Carboniferous Baizuo Fm., dolostone	−1.8	+23.6	
YCP2-A	Whole-rock	Lower Carboniferous Baizuo Fm., dolostone	+0.8	+21.0	
HE02	Whole-rock	Lower Carboniferous Baizuo Fm., dolostone	+0.1	+22.6	
HE12	Whole-rock	Lower Carboniferous Baizuo Fm., dolostone	−1.1	+21.1	
Qs-01	Whole-rock	Upper Carboniferous Maping Fm., dolostone	+2.3	+23.3	Mao et al. (1998)
Qs-04	Whole-rock	Upper Carboniferous Maping Fm., dolostone	+1.1	+22.1	
S-0	Whole-rock	Upper Carboniferous Huanglong Fm., limestone	+2.4	+25.5	
Sh-S-51	Whole-rock	Upper Carboniferous Huanglong Fm., limestone	+3.9	+26.8	
SI-9	Stage IV calcite	Upper Carboniferous Huanglong Fm., dolostone	+2.5	+25.6	
SSL7	Stage IV calcite	Upper Carboniferous Huanglong Fm., dolostone	+2.3	+26.5	This paper
SSL2	Stage I calcite	Sulfide ore	−1.6	+19.2	
SSL5	Stage I calcite	Sulfide ore	−1.4	+18.8	
SSL8	Stage I calcite	Sulfide ore	−1.7	+19.0	
SSL12-@4	Stage II calcite	Sulfide ore	−1.6	+19.5	
SSL14-@3	Stage II calcite	Sulfide ore	−1.9	+19.8	
SSL17-@4	Stage II calcite	Sulfide ore	−2.2	+20.3	
SSL13-@3	Stage III calcite	Sulfide ore	−3.1	+20.2	

be due to samples collected from different locations in this and previous studies. In addition, compared with the Huize (+10 to +18‰; Han et al., 2007a), Tianqiao (+8 to +14‰; Zhou et al., 2013a), Shaojiwan (+8 to +11‰; Zhou et al., 2013b) and Qingshan (+11 to +19‰; Zhou et al., 2013c) deposits, the sulfides from the Shanshulin deposit have higher $\delta^{34}S$ values (Fig. 8A).

5.3. Zinc isotopic compositions

Zinc isotopic compositions of sphalerite separates from the Shanshulin deposit and the country whole-rock samples are listed in Table 4 and shown in Fig. 9. Sphalerite from the Shanshulin deposit yields $\delta^{66}Zn$ values ranging from 0.00 to +0.55‰, with a mean value of +0.25‰ (Table 4). Five brown sphalerite and seven brown–yellow sphalerite samples have $\delta^{66}Zn$ values ranging from 0.00 to +0.21‰ and +0.19 to +0.55‰ (Table 4), respectively. It is obvious that the brown–yellow sphalerite has higher zinc isotope values in the same hand specimen (Fig. 9). Stage I brown sphalerite samples have $\delta^{66}Zn$ values ranging from 0.00 to +0.07‰ (average +0.04‰, n = 2). The $\delta^{66}Zn$ values of Stage II brown and brown–yellow sphalerite samples range from +0.12 to +0.23‰ (average +0.18‰, n = 5). Stage III brown–yellow sphalerite samples have $\delta^{66}Zn$ values ranging from +0.29 to +0.55‰ (average +0.40‰, n = 5). It is clear that the Stage III brown–yellow sphalerite has higher $\delta^{66}Zn$ values (Fig. 9). Compared with Devonian to Lower Permian sedimentary rocks (−0.22 to +0.17‰) and Middle Permian Emeishan flood basalts (+0.30 to +0.44‰; Zhou et al., 2014), sphalerite separates from the Shanshulin deposit have a wider range of $\delta^{66}Zn$ values (Fig. 9).

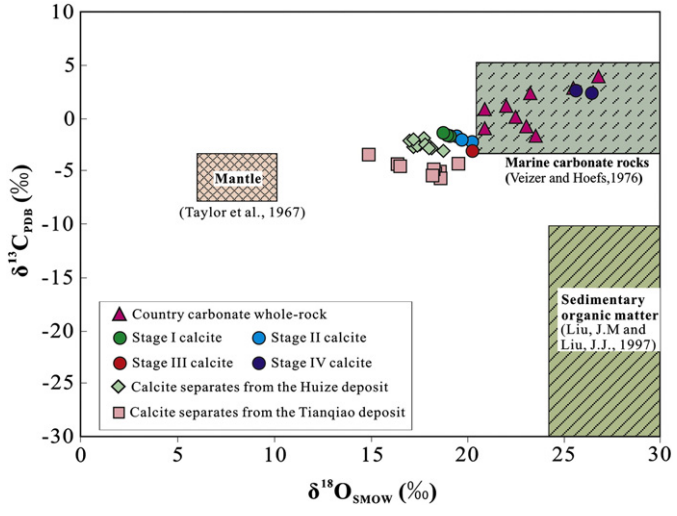

Fig. 7. Plot of $\delta^{13}C_{PDB}$ vs. $\delta^{18}O_{SMOW}$ for calcite and country carbonate whole-rock from the Shanshulin deposit area. Data for country carbonate whole-rock are from Hu (1999) and Mao et al. (1998); the Tianqiao deposit data are from Zhou et al. (2013a); the Huize deposit data are from Huang et al. (2010).

5.4. Lead isotopic compositions

Lead isotopic compositions of ores and sulfides from the Shanshulin Pb–Zn deposit and the country whole-rock samples are listed in Tables 5 and 6 and shown in Fig. 10. Four galena samples have $^{206}Pb/^{204}Pb$ ratios ranging from 18.531 to 18.573, $^{207}Pb/^{204}Pb$ ratios ranging from 15.722 to 15.769 and $^{208}Pb/^{204}Pb$ ratios ranging from 39.069 to 39.223 (Table 5). $^{206}Pb/^{204}Pb$, $^{207}Pb/^{204}Pb$ and $^{208}Pb/^{204}Pb$ ratios for seven sphalerite samples range from 18.362 to 18.567, 15.505 to 15.754 and 38.302 to 39.179, respectively (Table 5). It is obvious that Stage III sulfides contain more radiogenic Pb than Stage II and galena contains more radiogenic Pb than sphalerite (Fig. 10). The Pb isotope data are similar to previously reported data with the exception of a narrower range of $^{207}Pb/^{204}Pb$ ratios (Fig. 10). All the Pb isotope data are similar to the Huize (Han et al., 2007a) and Tianqiao (Zhou et al., 2013a) deposits (Fig. 10), suggesting a similar source for Pb.

5.5. Strontium isotopic compositions

The Sr isotope data of seven brown–yellow sphalerite and the country whole-rock samples are listed in Tables 7 and 8 and shown in Fig. 11. Sphalerite samples have very low contents of Rb (0.021 to 0.072 ppm) and a medium range of Sr concentrations (2.07 to 10.89 ppm). The $^{87}Rb/^{86}Sr$ ratios of the seven brown–yellow sphalerite samples range from 0.0190 to 0.0473 and the $^{87}Sr/^{86}Sr$ ratios range from 0.7108 to 0.7116 (Table 7). There is no difference in $^{87}Sr/^{86}Sr$ ratios between Stage II and Stage III brown–yellow sphalerite samples (Table 7). Limited variations in Sr isotopic compositions suggest that all sphalerite samples from the Shanshulin deposit have a uniform Sr source. Compared with the Huize (Han et al., 2007a) and Tianqiao (Zhou et al., 2013a) deposits, sphalerite separates from the Shanshulin deposit contain less radiogenic Sr (Fig. 11).

6. Discussion

6.1. Possible causes of zinc isotope variations

Significant variations were reported in the $\delta^{66}Zn$ values of sphalerite separates from the sediment-hosted Pb–Zn deposits of Cévennes in France (Albarède, 2004), Navan and Midlands in Ireland (Gagnevin

Table 3
Sulfur isotopic compositions of sulfide separates from the Shanshulin Pb–Zn deposit.

No.	Minerals	$\delta^{34}S_{CDT}$/‰	Sources	No.	Minerals	$\delta^{34}S_{CDT}$/‰	Sources
SS07	Py	+17.6	Fu (2004)	SS01	BY Sp	+17.2	Fu (2004)
78–59	Sp	+16.3	Chen (1986)	SS03	BY Sp	+17.5	
78–80	Sp	+16.1		SS14-1-@1	BY Sp	+18.4	
S3	Sp	+17.0		SS16	B Sp	+18.6	
S12	Sp	+18.3		78–79	Gal	+13.4	Chen (1986)
78–66	Sp	+15.9		78–64	Gal	+13.4	
SSL6-@1	Stage III BY Sp	+19.6	This paper	S11	Gal	+13.6	
SSL17-@1	Stage II B Sp	+19.3		A1159-S-4	Gal	+13.7	
SSL14-@2	Stage II BY Sp	+19.0		SSL17-@3	Stage II Gal	+15.8	This paper
SSL13-@2	Stage III BY Sp	+18.9		SSL12-@3	Stage II Gal	+15.7	
SSL1-@2	Stage II B Sp	+20.3		SSL6-@2	Stage III Gal	+17.1	
SSL12-@1	Stage II B Sp	+19.1		SSL10	Stage III Gal	+15.6	
SSL11	Stage III BY Sp	+19.2		SS14-1-@2	Gal	+14.2	Fu (2004)
SS13-@1	BY Sp	+18.7	Fu (2004)	SS14-@2	Gal	+14.1	
SS14-@2	BY Sp	+18.7		SS13-@2	Gal	+13.9	
No.	Mineral pairs	$\Delta\delta^{34}S$/‰	T (°C)	No.	Mineral pairs	$\Delta\delta^{34}S$/‰	T (°C)
SSL6	Sphalerite–galena	+2.5	292	SSL12	Sphalerite–galena	+3.4	211
SSL17	Sphalerite–galena	+3.5	204	SS13	Sphalerite–galena	+4.8	135
SS14	Sphalerite–galena	+4.6	143	SS14-1	Sphalerite–galena	+4.2	163

Py, pyrite; Sp, sphalerite; BY Sp, brown–yellow sphalerite; B Sp, brown sphalerite; Gal, galena.

et al., 2012; Wilkinson et al., 2005), Red Dog in the USA (Kelley et al., 2009) and Tianqiao–Banbanqiao in China (Zhou et al., 2014), as well as the volcanic-hosted massive sulfide deposit of Alexandrinka in Russia (Mason et al., 2005). These studies indicate that the earliest sphalerite precipitated from the hydrothermal systems was enriched in light zinc isotopes, followed by precipitation of sphalerite with progressively heavier isotopic compositions. Based on the spatial and temporal variations of zinc isotopic compositions, it is believed that variations in the sources of zinc were unlikely key controls (Archer et al., 2004; Gagnevin et al., 2012; John et al., 2008; Kelley et al., 2009; Maréchal and Sheppard, 2002; Mason et al., 2005; Wilkinson et al., 2005; Zhou et al., 2014). Three causes are proposed to explain the evolution from light to heavy zinc isotopes: (i) temperature gradients (Mason et al., 2005; Toutain et al., 2008), (ii) mixing of multiple zinc sources (Wilkinson et al., 2005), and (iii) fractional crystallization (Gagnevin et al., 2012; Kelley et al., 2009; Zhou et al., 2014).

Studies show that at low to medium temperatures (<300 °C), no correlation exists between $\delta^{66}Zn$ values and temperatures, either experimentally (30 to 50 °C; Maréchal and Sheppard, 2002) or within hydrothermal systems (60 to 250 °C; Wilkinson et al., 2005). However, at high temperatures (>300 °C), a systematic increase in $\delta^{66}Zn$ values (−0.03 to +0.23‰) away from the hydrothermal vent (c. 300 °C) in Alexandrinka volcanic-hosted massive sulfide (VHMS) ore deposit, Urals, Russia was reported (Mason et al., 2005). Furthermore, a Rayleigh condensation model with temperature dependent Zn isotope fractionation ($1000\ln\alpha_{solid/vapor} = C_1 + C_2/T + C_3/T^2$, with $C_1 = 0$,

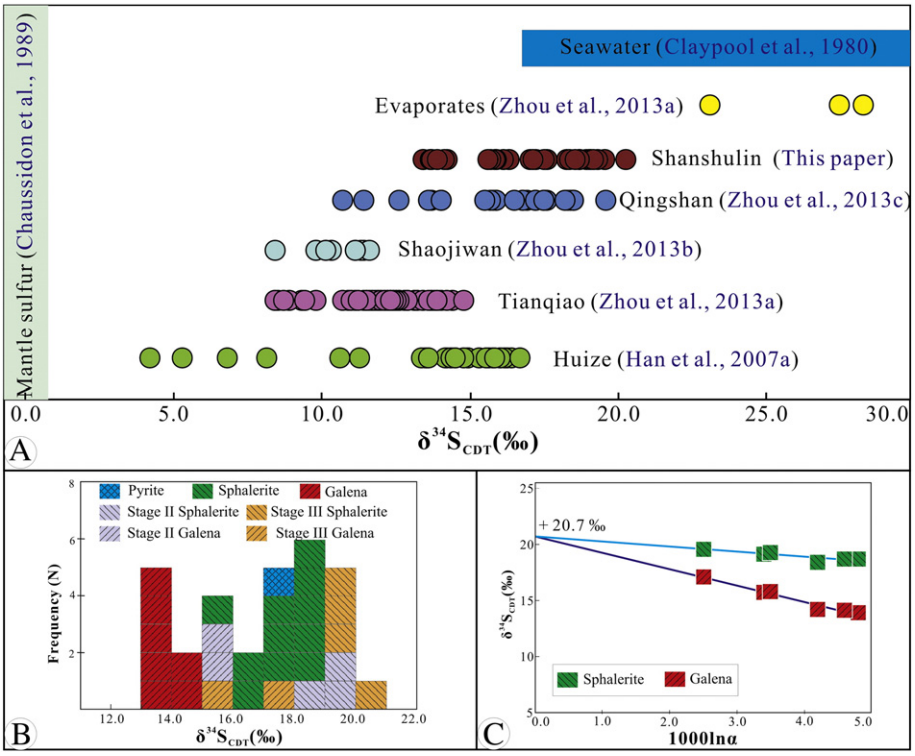

Fig. 8. A: The $\delta^{34}S_{CDT}$ values for the Shanshulin deposit are compared with those of mantle, seawater and evaporates, and the Huize, Tianqiao, Shaojiwan and Qingshan deposits; B: sulfur isotopic composition histogram of the Shanshulin Pb–Zn deposit; C: plot of $\delta^{34}S_{CDT}$ vs. 1000lnα for symbiotic sphalerite–galena mineral pairs.

Table 4
Zinc isotopic compositions of sphalerite separates from the Shanshulin deposit and of whole-rock of Devonian to Lower Permian sedimentary rocks and Middle Permian Emeishan flood basalts.

No.	Mineral/rock	Positions	$\delta^{66}Zn_{JMC,‰}$ [a]	SD	NA
SSL1-@1	Stage III BY Sp	Tunnel 23, 1820 m	0.30	0.04	3
SSL1-@1 [b]	Stage III BY Sp	Tunnel 23, 1820 m	0.29	0.05	2
SSL1-@2	Stage II B Sp	Tunnel 23, 1820 m	0.21	0.03	3
SSL6-@1	Stage III BY Sp	ZK248, 1590 m	0.49	0.07	2
SSL11	Stage III BY Sp	ZK63, 1660 m	0.31	0.05	2
SSL12-@1	Stage II BY Sp	Tunnel 25, 1770 m	0.19	0.04	3
SSL12-@2	Stage I B Sp	Tunnel 25, 1770 m	0.00	0.06	3
SSL13-@1	Stage II B Sp	Tunnel 27, 1700 m	0.12	0.07	4
SSL13-@2	Stage III BY Sp	Tunnel 27, 1700 m	0.35	0.05	3
SSL14-@1	Stage I B Sp	ZK63, 1670 m	0.07	0.05	2
SSL14-@2	Stage II BY Sp	ZK63, 1670 m	0.23	0.04	2
SSL17-@1	Stage II B Sp	ZK248, 1580 m	0.14	0.05	4
SSL17-@2	Stage III BY Sp	ZK248, 1580 m	0.55	0.08	2
D09-3	Sandstone	Middle Devonian Haikou Fm. [c]	−0.19	0.06	3
D09-5	Sandstone	Middle Devonian Haikou Fm. [c]	0.06	0.06	2
D09-7	Limestone	Upper Devonian Zaige Fm. [c]	−0.22	0.05	3
D22	Limestone	Lower Carboniferous Dapu Fm. [c]	−0.12	0.04	3
D23	Dolostone	Lower Carboniferous Baizuo Fm. [c]	0.15	0.04	3
D24	Dolostone	Lower Carboniferous Baizuo Fm. [c]	0.17	0.05	3
D09-10	Shale	Lower Permian Liangshan Fm. [c]	−0.16	0.06	3
Ems09-14	Basalts	Middle Permian Emeishan Fm. [c]	0.32	0.06	3
Ems09-15	Basalts	Middle Permian Emeishan Fm. [c]	0.30	0.04	3
Ems09-16	Basalts	Middle Permian Emeishan Fm. [c]	0.44	0.10	3

BY Sp, brown–yellow sphalerite; B Sp, brown sphalerite; Fm., Formation; SD, standard deviation; NA, number of analyses.
Samples SSL1-@1 and SSL1-@2 are from the same hand specimen SSL1; similarly, SSL12-@1 and SSL12-@2 from SSL12; SSL13-@1 and SSL13-@2 from SSL13; SSL14-@1 and SSL14-@2 from SSL14; SSL17-@1 and SSL17-@2 from SSL17.
[a] Mean over n number of repeats.
[b] Samples are used for procedural repeats.
[c] Zinc isotopic data of Devonian to Lower Permian sedimentary rocks and Middle Permian Emeishan flood basalts are taken from Zhou et al. (2014).

$C_2 = -0.88 \times 10^3$, $C_3 = 1.00 \times 10^6$ and T in degree Kelvin) was used to explain the significant difference between $\delta^{66}Zn$ values in fumarolic gases (+0.05 to +0.85‰) and condensates (+1.48 to +1.68‰) in the Woro fumarolic (590 to 297 °C) field, Merapi volcano, Indonesia (Toutain et al., 2008). Previous studies on the homogenization temperatures of fluid inclusions (150 to 280 °C; Fu, 2004) from the Shanshulin deposit indicate that the fluids which formed the deposit were low to medium temperatures (<300 °C). Sulfide formation temperatures calculated as part of this study (see below) are consistent with temperatures less than 300 °C. Therefore, temperature gradient is likely not a key factor in the observed Zn isotope variations (Fig. 9). In the SYG province, the whole-rock samples of Devonian to lower Permian sedimentary rocks and Middle Permian Emeishan flood basalts have $\delta^{66}Zn$ values ranging from −0.22 to +0.17‰ and +0.30 to +0.44‰, respectively (Zhou et al., 2014). These values are narrower than sphalerite separates from the Shanshulin deposit (Fig. 9), thus precluding

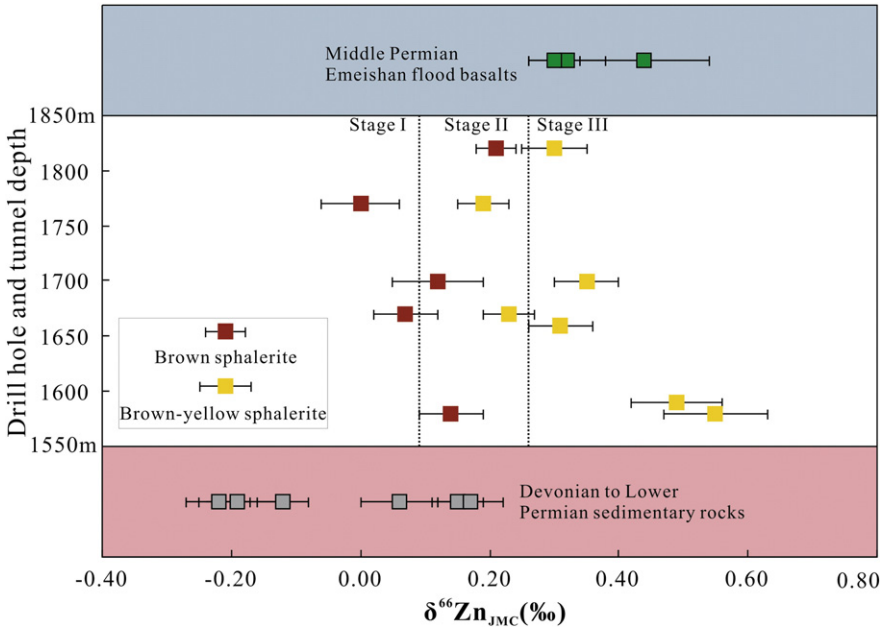

Fig. 9. Zinc isotopic variations for sphalerite separates from the Shanshulin deposit. The variations among three stages represent temporal differences. Spatial differences are represented with depth (in meters). The zinc isotopic compositions of sphalerite samples from the Shanshulin deposit are compared with those of whole-rock of Middle Permian Emeishan flood basalts and Devonian to Lower Permian sedimentary rocks (Zhou et al., 2014).

Table 5
Lead isotopic compositions of ores and sulfide separates from the Shanshulin Pb–Zn deposit.

No.	Mineral/ore	$^{206}Pb/^{204}Pb$	$^{207}Pb/^{204}Pb$	$^{208}Pb/^{204}Pb$	Sources	No.	Mineral/ore	$^{206}Pb/^{204}Pb$	$^{207}Pb/^{204}Pb$	$^{208}Pb/^{204}Pb$	Sources
SS01	BY Sp	18.503	15.726	38.970	Fu (2004)	SSL1-@1	Stage III BY Sp	18.412	15.561	38.452	This paper
SS03	BY Sp	18.593	15.802	39.300		SSL11	Stage III BY Sp	18.441	15.559	38.601	
SS13	BY Sp	18.530	15.709	39.041		SSL14-@2	Stage II BY Sp	18.428	15.601	38.558	
SS14-@1	BY Sp	18.528	15.710	39.024		SSL17-@1	Stage II B Sp	18.362	15.515	38.302	
SS14-1-@1	BY Sp	18.474	15.657	38.881		SSL13-@2	Stage III BY Sp	18.395	15.505	38.312	
SS16	B Sp	18.510	15.687	38.957		SS101	Ore	18.551	15.755	39.255	Zheng (1994);
SS07	Py	18.506	15.677	38.915		S3117	Ore	18.495	15.701	39.016	Zhang et al. (1998)
SS14-@2	Gal	18.596	15.798	39.332		S4115	Ore	18.499	15.681	38.965	
SS14-1-@2	Gal	18.654	15.874	39.573		S5137-3	Ore	18.496	15.705	39.083	
Pb-73	Gal	18.278	15.448	38.545	Liu and Lin (1999)	S5127-2	Ore	18.493	15.757	39.185	
Pb-74	Gal	18.276	15.457	38.553		Ssl001	Gal	18.619	15.742	39.345	
Pb-78	Gal	18.450	15.605	38.687		Ssl002	Gal	18.546	15.716	39.264	
TzPb1	Gal	18.475	15.675	38.924		23y-3003	Gal	18.336	15.458	39.304	
TzPb2	Gal	18.502	15.698	39.012		26k	Gal	18.490	15.610	38.980	
TzPb3	Gal	18.457	15.684	38.846		81093	Gal	18.472	15.673	38.923	
S26	Gal	18.488	15.607	38.977		81094	Gal	18.512	15.696	39.018	
33-Y3003	Gal	18.335	15.551	38.299		81095	Gal	18.547	15.864	38.845	
SSL6-@2	Stage III Gal	18.573	15.769	39.223	This paper	SA1150-1	Gal	18.471	15.648	38.455	
SSL17-@3	Stage II Gal	18.552	15.743	39.141		SA1150–2	Gal	18.481	15.657	38.553	
SSL10	Stage III Gal	18.556	15.756	39.194		75g-1	Gal	18.452	15.625	38.679	
SSL12-@3	Stage II Gal	18.531	15.722	39.069		S3317	Gal	18.491	15.702	39.006	
SSL12-@1	Stage II BY Sp	18.549	15.736	39.117		S5237	Gal	18.539	15.705	38.083	
SSL6-@1	Stage III BY Sp	18.567	15.754	39.179		S5137-2	Gal	18.613	15.775	39.103	

Py, pyrite; BY Sp, brown–yellow sphalerite; B Sp, brown sphalerite; Gal, galena.

the mixing of multiple zinc sources as a key factor in controlling the variations in zinc isotopic compositions (Fig. 9). Fractional crystallization has been used to explain an increase of $\delta^{66}Zn$ values from the early to late stages of sulfide deposition (Gagnevin et al., 2012; Kelley et al., 2009; Mason et al., 2005; Wilkinson et al., 2005; Zhou et al., 2014). Brown sphalerite preceded precipitation of brown–yellow sphalerite in the Shanshulin deposit, and because the Zn isotope compositions follow the trend from lighter to heavier (Fig. 9), it follows that kinetic Rayleigh fractionation was likely responsible for the observed Zn isotopic variations. Moreover, similar to the sphalerite separates from the Cévennes (−0.06 to +0.42‰; Albarède, 2004), Midlands (−0.17 to +0.64‰, with one value at +1.33‰; Wilkinson et al., 2005) and Navan (−0.32 to +0.23‰; Gagnevin et al., 2012) MVT-type deposits in Europe, the Alexandrinka VHMS-type deposit in Russia (−0.43 to +0.23‰; Mason et al., 2005) and the Red Dog SEDEX-type deposit in the USA (0.00 to +0.60‰; Kelley et al., 2009), those from the Shanshulin Pb–Zn deposit do not have unique Zn isotope values (Fig. 12). This suggests that Zn isotopes may not be suitable for discriminating ore genesis.

6.2. Source of ore-forming fluids

In general terms, there are three principal sources of C–O in hydrothermal fluid: (i) mantle, (ii) marine carbonate rocks, and (iii) sedimentary organic matter (Demény and Harangi, 1996; Demény et al., 1998; Liu, J.M. and Liu, J.J., 1997; Taylor et al., 1967; Veizer and Hoefs, 1976). The $\delta^{13}C_{PDB}$ and $\delta^{18}O_{SMOW}$ values for mantle, marine carbonate and organic matter range from −4.0 to −8.0‰ and +6.0 to +10.0‰ (Taylor et al., 1967), −4.0 to +4.0‰ and +20.0 to +30.0‰ (Veizer and Hoefs, 1976), and −30.0 to −10.0‰ and +24.0 to +30.0‰ (Liu, J.M. and Liu, J.J., 1997), respectively. Calcite samples from the Shanshulin deposit have $\delta^{13}C_{PDB}$ values higher than mantle and organic matter, but similar to those of marine carbonate and the carbonate country rocks (Fig. 7). This indicates that mantle and organic matter did not contribute significant quantities of C to the hydrothermal fluids. The similarity of $\delta^{13}C_{PDB}$ and $\delta^{18}O_{SMOW}$ values in calcite samples and the country whole-rock suggest that C and O isotopes in the hydrothermal fluid were nearly in thermal equilibrium with the country rocks (Gray et al., 1991; Muchez et al., 1995). Therefore, the carbon and oxygen in the ore-forming fluid were likely provided by the carbonate country rocks. Calcite separates from the Huize (Huang et al., 2010) and Tianqiao (Zhou et al., 2013a) deposits have $\delta^{18}O_{SMOW}$ values lower than that from the Shanshulin deposit which suggests oxygen in the formers was likely derived from an ^{18}O-depleted source region.

Sulfide ores in the Shanshulin deposit have simple S-bearing mineralogy, including sphalerite, pyrite and galena, but they lack sulfate. Therefore, the $\delta^{34}S$ values of sulfide minerals (especially pyrite) approximate the hydrothermal fluid's $\delta^{34}S$ values (e.g. Basuki et al., 2008; Dixon and Davidson, 1996; Ohmoto and Goldhaber, 1997; Ohmoto and Rye, 1979; Ohmoto et al., 1990). One pyrite sample from the

Table 6
Pb isotopic compositions for the Tianqiao and Huize deposits, Devonian to Lower Permian carbonate rocks, Proterozoic folded basement rocks and Middle Permian Emeishan flood basalts.

Mineral/rock	Number	$^{206}Pb/^{204}Pb_{200\ Ma}$	$^{207}Pb/^{204}Pb_{200\ Ma}$	$^{208}Pb/^{204}Pb_{200\ Ma}$
Tianqiao deposit sulfides	33	18.378–18.601	15.519–15.811	38.666–39.571
Huize deposit sulfides	95	18.251–18.530	15.439–15.855	38.487–39.433
Middle Permian Emeishan flood basalts whole-rock	56	18.175–19.019	15.528–15.662	38.380–39.928
Lower Permian Qixia Fm., limestone whole-rock	12	18.189–18.759	15.609–16.522	38.493–38.542
Upper Carboniferous Huanglong Fm., limestone whole-rock	12	18.136–18.167	15.656–16.675	38.204–38.236
Lower Carboniferous Baizuo Fm., dolostone whole-rock	28	18.120–18.673	15.500–16.091	38.235–39.685
Lower Carboniferous Dapu Fm., dolostone whole-rock	15	18.397–18.828	15.537–16.499	38.463–39.245
Upper Devonian Zaige Fm., limestone whole-rock	13	18.245–18.842	15.681–16.457	38.715–39.562
Proterozoic basement whole-rock (Kunyang and Huili Groups)	43	17.781–20.993	15.582–15.985	37.178–40.483

Pb isotopic compositions for the Huize deposit are from Han et al. (2007a) and Zhou et al. (2001), and for the Tianqiao deposit are from Zhou et al. (2013a). Other data are from Fu (2004), Han et al. (2007a), Hu (1999), Huang et al. (2004), Liu and Lin (1999), Zhang et al. (1998), Zheng and Wang (1991) and Zhou et al. (2001, 2013a, 2013d). $^{206}Pb/^{204}Pb_t = {}^{206}Pb/^{204}Pb_p\text{-}\mu(e^{\lambda t}-1)$, $^{207}Pb/^{204}Pb_t = {}^{207}Pb/^{204}Pb_p\text{-}\mu/137.88(e^{\lambda t}-1)$, $^{208}Pb/^{204}Pb_t = {}^{208}Pb/^{204}Pb_p\text{-}\omega(e^{\lambda'' t}-1)$, $\lambda = 1.55125 \times 10^{-10}\ t^{-1}$, $\lambda' = 9.8485 \times 10^{-10}\ t^{-1}$, $\lambda'' = 0.49475 \times 10^{-10}\ t^{-1}$, $t = 200$ Ma.

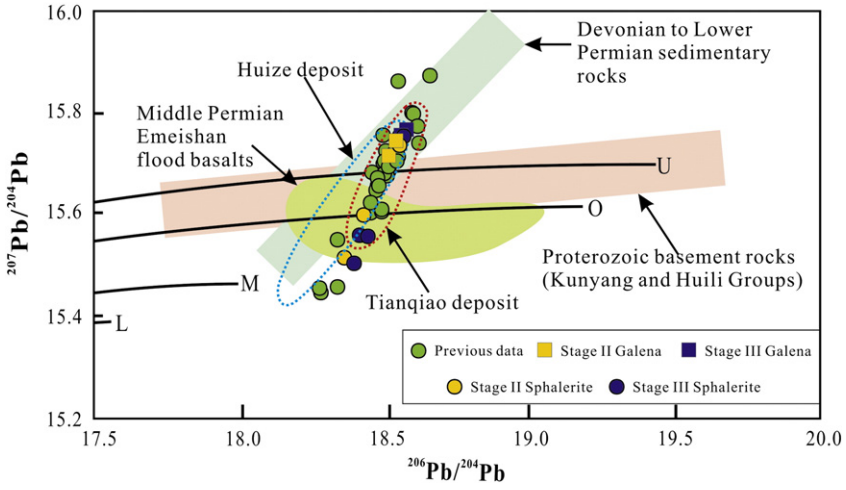

Fig. 10. Plot of $^{207}Pb/^{204}Pb$ vs. $^{206}Pb/^{204}Pb$ for sulfide minerals from the Shanshulin Pb–Zn deposit, including those from previous studies (Fu, 2004; Liu and Lin, 1999; Zhang et al., 1998; Zheng, 1994). Comparison is made with bulk ore compositions from Zhang et al. (1998) and Zheng (1994). Trends for the upper crust (U), orogenic belt (O), mantle (M) and lower crust (L) are from Zartman and Doe (1981). Data from the Huize and Tianqiao deposits, and bulk-rock Pb isotopic compositions are from Fu (2004), Han et al. (2007a), Hu (1999), Huang et al. (2004), Liu and Lin (1999), Zhang et al. (1998), Zheng and Wang (1991) and Zhou et al. (2001, 2013a, 2013d) and are age-corrected at 200 Ma.

Shanshulin deposit has a $\delta^{34}S_{CDT}$ value of +17.6‰ (Table 3; Fu, 2004), which is significantly higher than that of mantle-derived magmatic sulfur (0 ± 3‰; Chaussidon et al., 1989). Because rigorous interpretation is not possible due to the paucity of data for pyrite, the $\delta^{34}S_{fluid}$ value was calculated by paragenetic sphalerite–galena sulfide pairs (Pinckney and Rafter, 1972). The resulting value of +20.7‰ for the fluid (Fig. 8C) is similar to that of pyrite. Devonian to Lower Permian sedimentary rocks in the southeast SYG province contain evaporites such as gypsum and barite that have $\delta^{34}S_{CDT}$ values range from +22 to +28‰, (Jin, 2008; Liu and Lin, 1999; Zhou et al., 2013a), similar to those of Devonian to Permian seawater (+15 to +25‰; Claypool et al., 1980; Seal, 2006). The temperature of S isotope equilibrium fractionation may be calculated using sulfide mineral pairs. The $\Delta\delta^{34}S_{sphalerite-galena}$ values of six sphalerite–galena pairs range from +2.5 to +4.8‰ (Table 3), suggesting possible deposition of sulfide minerals under S isotope equilibrium conditions. Assuming sulfide precipitation under thermal equilibrium conditions, the observed fractionation for the six sphalerite–galena pairs in the Shanshulin deposit corresponds to ore-forming temperatures of 135 to 292 °C (Table 3; Czamanske and Rye, 1974). These calculated temperatures are similar to the homogenization temperatures derived from the previous fluid inclusion studies (150 to 280 °C; Fu, 2004), but are higher than those of bacterial sulfate reduction (BSR) (Basuki et al., 2008; Dixon and Davidson, 1996; Jorgenson et al., 1992; Machel et al., 1995), which could result in a larger sulfur isotopic fractionation (in an open system). Therefore, the origin of reduced sulfur in hydrothermal fluids from the Shanshulin deposit was likely thermo-chemical sulfate reduction (TSR), which is in agreement with the interpretation of the Huize (Han et al., 2007a) and Tianqiao (Zhou et al., 2013a) deposits.

6.3. Origin of ore-forming elements

U and Th contents of sulfide minerals are too low to influence their Pb isotopic composition, whereas the Pb isotopic compositions of Proterozoic folded basement rocks, Devonian to Lower Permian sedimentary rocks and Middle Permian Emeishan flood basalts must be corrected for age (e.g. Carr et al., 1995; Haest et al., 2010; Muchez et al., 2005; Zhang et al., 2002). Studies in the SYG province show that the ages of Pb–Zn mineralization are between 222 and 192 Ma (Li et al., 2007b; Lin et al., 2010; Mao et al., 2012; Zhou et al., 2013a, 2013d). Thus, an age of 200 Ma is used to correct the Pb isotopic compositions of the country rocks. In terms of $^{207}Pb/^{204}Pb$ vs. $^{206}Pb/^{204}Pb$ ratios (Fig. 10), all data of the Shanshulin deposit show a linear correlation that crosscuts the upper crust, orogenic belt and mantle Pb evolution curves (Zartman and Doe, 1981), suggesting a mixture of Pb sources in hydrothermal fluid. Moreover, Pb isotope data for samples from the Shanshulin deposit plot crosscut the age-corrected Proterozoic basement, Devonian to Lower Permian sediment and Middle Permian basalts (Table 6; Fig. 10). This suggests that the Pb in the ore-forming fluid may have had multiple sources, presumably including basement, sedimentary rocks and basalts in the SYG province.

In order to use Sr isotopic compositions of hydrothermal minerals to trace the source of ore-forming metals, there needs to be an age correction (e.g. Deng et al., 2000; Fontbote and Gorzawski, 1990; Gromek et al., 2012; Zhou et al., 2001). Therefore, the 200 Ma sulfide formation age was used to correct the $^{87}Sr/^{86}Sr$ ratios of sphalerite separates from the Shanshulin deposit, and the basement, sedimentary rocks and basalts in the SYG province. The $^{87}Sr/^{86}Sr_{200\ Ma}$ ratios of Lower Permian Qixia Formation limestone and Lower Carboniferous Baizuo Formation

Table 7
Rb–Sr isotopic compositions of sphalerite separates from the Shanshulin Pb–Zn deposit.

No.	Mineral	Rb/ppm(10^{-6})	Sr/ppm(10^{-6})	$^{87}Rb/^{86}Sr$	$^{87}Sr/^{86}Sr$	$^{87}Sr/^{86}Sr_{200\ Ma}$	Source
SSL1-@1	Stage III BY Sp	0.072	10.89	0.0190	0.7116	0.7115	This paper
SSL6-@1	Stage III BY Sp	0.038	3.27	0.0332	0.7108	0.7107	
SSL11	Stage III BY Sp	0.031	3.14	0.0315	0.7111	0.7110	
SSL12-@1	Stage II BY Sp	0.021	2.07	0.0296	0.7116	0.7115	
SSL13-@2	Stage III BY Sp	0.021	2.64	0.0229	0.7115	0.7114	
SSL14-@2	Stage II BY Sp	0.050	3.08	0.0473	0.7115	0.7114	
SSL17-@2	Stage III BY Sp	0.022	3.00	0.0212	0.7114	0.7113	

BY Sp, brown–yellow sphalerite. $(^{87}Sr/^{86}Sr)_t = {}^{87}Sr/^{86}Sr - {}^{87}Sr/^{87}Rb\ (e^{\lambda t}-1)$, $\lambda_{Rb} = 1.41 \times 10^{-11} t^{-1}$, t = 200 Ma.

Table 8
Strontium isotopic compositions of sulfide separates from the Shanshulin, Tianqiao and Huize deposits, and of whole-rock of Proterozoic basement rocks, Devonian to Lower Permian sedimentary rocks, Middle Permian Emeishan flood basalts and the Upper Mantle.

Mineral/rock	Num.	$^{87}Sr/^{86}Sr_{200\ Ma}$		Sources
		Range	Average	
Sphalerite from the Shanshulin deposit	7	0.7107–0.7115	0.7113	This paper
Sphalerite and pyrite from the Tianqiao deposit	7	0.7118–0.7130	0.7124	Zhou et al. (2013a)
Hydrothermal minerals from the Huize deposit	35	0.7137–0.7170	0.7163	Huang et al. (2004)
Lower Permian Qixia Fm., limestone	1	0.7079	0.7075	Deng et al. (2000)
	1	0.7075		This paper
	1	0.7073		
Upper Carboniferous Maping Fm., limestone	2	0.7099–0.7100	0.7100	Zhou et al. (2013a)
Lower Carboniferous Baizuo Fm., dolostone	3	0.7087–0.7093	0.7091	Hu (1999)
	1	0.7099		This paper
	1	0.7101	0.7101	
Upper Devonian Zaige Fm., limestone	2	0.7084–0.7088	0.7086	Zhou et al. (2013a)
Middle Devonian Qujing Fm., dolostone	1	0.7101	0.7101	Deng et al. (2000)
Middle Devonian Haikou Fm., sandstone	1	0.7111	0.7111	Zhou et al. (2013a)
Middle Permian Emeishan flood basalts	85	0.7039–0.7078	0.7058	Huang et al. (2004)
Proterozoic folded basement rocks (Kunyang/Huili Groups)	5	0.7243–0.7288	0.7268	Li and Qin (1988); Chen and Ran (1992)
Upper Mantle		0.704 ± 0.002	0.704	Faure (1977)

$(^{87}Sr/^{86}Sr)_t = {}^{87}Sr/^{86}Sr - {}^{87}Sr/^{87}Rb\ (e^{\lambda t} - 1)$, $\lambda_{Rb} = 1.41 \times 10^{-11} t^{-1}$, $t = 200$ Ma.

dolostone range from 0.7073 to 0.7075 and 0.7099 to 0.7101, respectively (Table 8), similar to previously reported age-corrected Sr isotope values of Devonian to Lower Permian sedimentary rocks (0.7075 to 0.7111; Deng et al., 2000; Hu, 1999; Zhou et al., 2013a). In addition, the Sr isotopic compositions of sphalerite separates from the Shanshulin deposit are similar to Devonian to Lower Permian sedimentary rocks (0.7073 to 0.7111; Table 8), whereas they are higher than those in Middle Permian basalts (0.7039 to 0.7078; Huang et al., 2004). On the other hand, Proterozoic folded basement samples have $^{87}Sr/^{86}Sr_{200\ Ma}$ ratios ranging from 0.7243 to 0.7288 (Chen and Ran, 1992; Li and Qin, 1988), significantly higher than those of the sphalerite separates from the Shanshulin deposit (Table 8; Fig. 11). Neither the basement rocks nor the Devonian to Lower Permian sedimentary rocks and Middle Permian basalts match the sphalerite $^{87}Sr/^{86}Sr_{200\ Ma}$ ratios. Therefore, the sulfide strontium was likely sourced from a mixture of radiogenic Sr-enriched basement rocks and radiogenic Sr-depleted sedimentary rocks and basalts (Fig. 11), as suggested by Pb isotope data. The $^{87}Sr/^{86}Sr_{200\ Ma}$ ratios of sphalerite separates from the Shanshulin deposit range from 0.7107 to 0.7115, similar to those of sulfide minerals from the Tianqiao deposit (0.7118 to 0.7130; Zhou et al., 2013a), but lower than those of hydrothermal minerals from the Huize deposit (0.7137 to 0.7170; Huang et al., 2004), suggesting that the radiogenic Sr-enriched Proterozoic folded basement rocks contributed significantly to the Sr of the Huize deposit (Tables 7 and 8; Fig. 11).

6.4. Ore genesis and prospecting

The ore deposits in the SYG province may have been affected by reworking and recrystallization, because of multiple orogenic episodes (e.g. Zaw et al., 2007). Due to these complexities, the ore genesis of these deposits has long been a matter of debate. For example, it has been proposed that all of the Pb–Zn deposits in the SYG province were distal magmatic-hydrothermal deposits (Xie, 1963) relative to the Middle Permian Emeishan flood basalts, while isotope chronology studies have suggested that the Pb–Zn deposits in the SYG province may have formed during the Late Triassic to Early Jurassic (222–192 Ma; Li et al., 2007b; Lin et al., 2010; Mao et al., 2012; Zhou et al., 2013a, 2013d), which is younger than the Middle Permian basalts (~260 Ma;

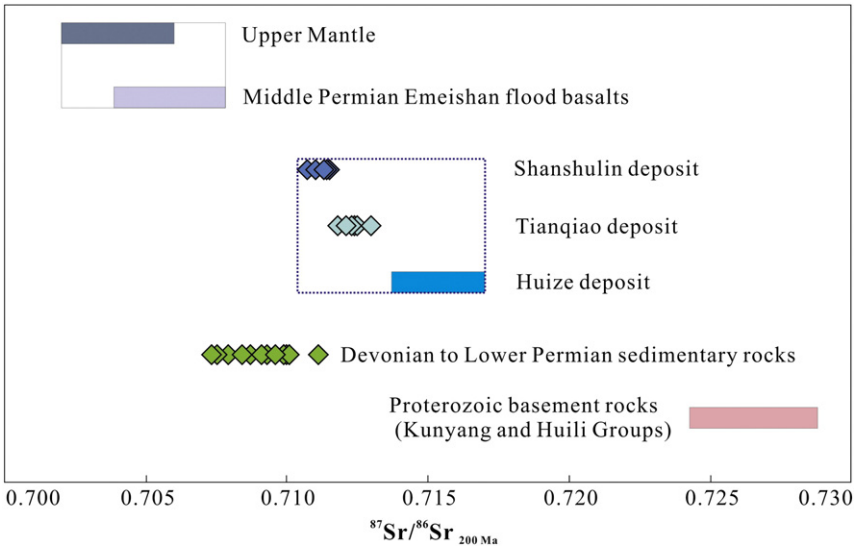

Fig. 11. Comparison of $^{87}Sr/^{86}Sr_{200\ Ma}$ ratios between the Shanshulin, Tianqiao and Huize Pb–Zn deposits, Proterozoic basement rocks, Devonian to Lower Permian sedimentary rocks, Middle Permian Emeishan flood basalts, and Upper Mantle (Faure, 1977). Data from the Huize and Tianqiao deposits, and whole-rock strontium isotope values are from this research and previous studies, including Chen and Ran (1992), Deng et al. (2000), Han et al. (2007a), Hu (1999), Huang et al. (2004), Li and Qin (1988) and Zhou et al. (2013a).

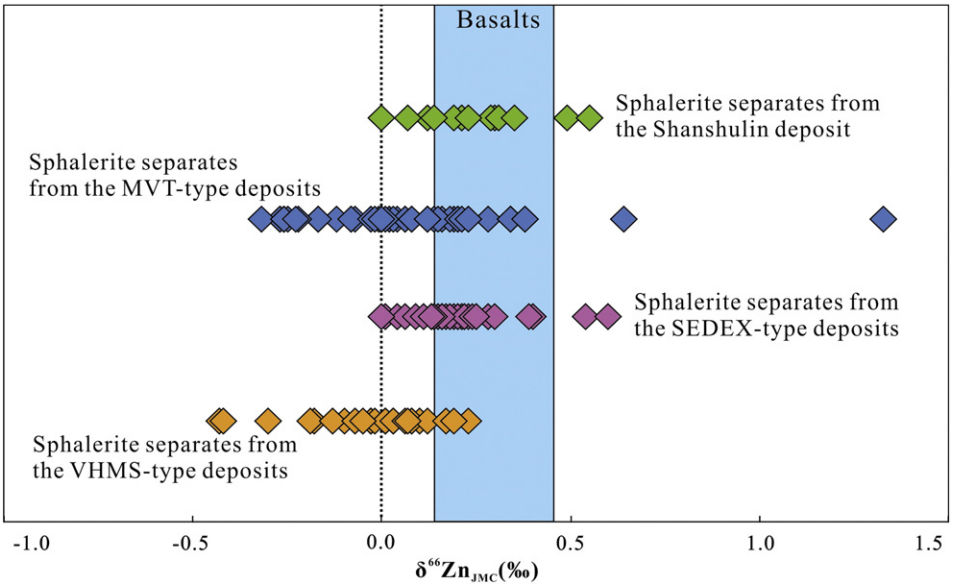

Fig. 12. Comparison of zinc isotopic compositions between sphalerite separates from the Shanshulin deposit and Pb–Zn deposits of MVT, SEDEX and VHMS-types. Zinc isotope data for MVT deposits are from Albarède (2004), Wilkinson et al. (2005) and Gagnevin et al. (2012), SEDEX-type from Kelley et al. (2009), and VHMS-type from Mason et al. (2005).

Zhou et al., 2002). It has also been suggested that the Pb–Zn deposits in the SYG province are comparable to typical MVT-type deposits (e.g. Leach et al., 2001, 2005, 2010; Muchez et al., 2005; Oliver, 1986, 1992; Pirajno, 2009, 2013) in terms of tectonic setting, type of host rocks and source of ore-forming fluids (Wang et al., 2000, 2003; Zaw et al., 2007; Zheng and Wang, 1991; Zhou et al., 2001). Nevertheless, these deposits display a set of characteristics that contrast with those of typical MVT-type deposits, including ore-controlled thrust faults, high grades of Pb + Zn metals, complex sources of ore-forming metals, simple wall rock alteration and the lack of collapse breccias (e.g. Han et al., 2007a; Zhou et al., 2013a, 2014). Although there is no direct genetic relationship between the Middle Permian basalts and Pb–Zn deposits, the basalts could have provided some of the Pb and Sr to the system, as suggested by our new Pb–Sr isotopic data. Therefore, an alternative model is that the Shanshulin deposit is a carbonate-hosted, strata-bound, epigenetic, thrust fault-controlled, high grade deposit formed by fluids and metals of mixed origin (e.g. Han et al., 2007a; Huang et al., 2010; Zhou et al., 2011, 2013a, 2013d). The mineralization process is similar to that of MVT-type deposits elsewhere, including extraction of ore-forming elements from basement and country rocks by convective circulation of hydrothermal fluids and subsequent precipitation of these elements in favorable structural and lithological units (Hu and Zhou, 2012; Zhou et al., 2001).

For the reason that ore bodies in the Shanshulin deposit occur along the thrust faults, the contact zone between dolomitic limestone and dolostone along the F_9 thrust fault is considered as an important target (Fig. 3). Furthermore, because the Zn isotope variations in the Shanshulin deposit are interpreted to represent fractional crystallization, with higher $\delta^{66}Zn$ values representing later stages of precipitation (and perhaps most distal from the core of the hydrothermal system), Zn isotope data may be considered an exploration tool (Kelley et al., 2009). If these assumptions are true, variations in Zn isotope values for sphalerite may provide clues for prospecting concealed ores in deep parts of the contact zone along the F_9 thrust fault in the Shanshulin deposit area (Fig. 3).

7. Conclusion

The Shanshulin Pb–Zn deposit is hosted by the Upper Carboniferous Huanglong Formation dolomitic limestone and dolostone, and occurs along the secondary high angle thrust faults of the Weishui fault. C–O and S stable isotopes suggest that carbon and sulfur in the hydrothermal fluid were derived from the country rocks. Pb and Sr radiogenic isotopes indicate that the ore lead and strontium were sourced from Proterozoic folded basement, Devonian to Lower Permian sedimentary rocks and Middle Permian Emeishan flood basalts. The later-precipitated brown–yellow sphalerite has heavier Zn isotopic compositions than the earlier deposited brown sphalerite. These variations may be explained by fractional crystallization and Zn isotopes may be considered as an exploration tool.

Acknowledgments

This research was financially supported by the National Basic Research Program of China (No. 2014CB440905) and the National Natural Science Foundation of China (Nos. 41102055 and 41272111). Thanks are given to Prof. Mei-Fu Zhou, Lin Ye and Taiyi Luo for their insightful suggestions. Comments and suggestions by Prof. Franco Pirajno (Editor-in-Chief), Karen Kelley and Philippe Muchez greatly improved the quality of the paper.

References

Albarède, F., 2004. The stable isotope geochemistry of copper and zinc. Rev. Mineral. Geochem. 55, 409–427.
Archer, C., Vance, D., Butler, I., 2004. Abiotic Zn isotope fractionations associated with ZnS precipitation. Geochim. Cosmochim. Acta 68, A325.
Basuki, N.I., Taylor, B.E., Spooner, E.T.C., 2008. Sulfur isotope evidence for thermochemical reduction of dissolved sulfate in Mississippi valley type zinc–lead mineralization, Bongara area, northern Peru. Econ. Geol. 103, 183–799.
Carr, G.R., Dean, J.A., Suppel, D.W., Heithersay, P.S., 1995. Precise lead isotope fingerprinting of hydrothermal activity associated with Ordovician to Carboniferous metallogenic events in the Lachlan fold belt of New South Wales. Econ. Geol. 90, 1467–1505.
Chaussidon, M., Albarède, F., Sheppard, S.M.F., 1989. Sulphur isotope variations in the mantle from ion microprobe analyses of micro-sulphide inclusions. Earth Planet. Sci. Lett. 92, 144–156.
Chen, S.J., 1986. A discussion on the origin of Pb–Zn deposits in western Guizhou and northeastern Yunnan. Guizhou Geol. 3, 211–222 (in Chinese with English abstract).
Chen, H.S., Ran, C.Y., 1992. Isotope Geochemistry of Copper Deposit in Kangdian Area. Geological Publishing House, Beijing pp. 1–25 (in Chinese).
Chen, J.B., Gaillardet, J., Dessert, C., Villemant, B., Louvat, P., Crispi, O., Birck, J.L., Wang, Y.N., 2013. Zn isotope compositions of the thermal spring waters of La Soufrière volcano, Guadeloupe Island. Geochim. Cosmochim. Acta 127, 67–82.
Claypool, G.E., Holser, W.T., Kaplan, I.R., Sakai, H., Zak, I., 1980. The age curves of sulfur and oxygen isotopes in marine sulfate and their mutual interpretation. Chem. Geol. 28, 199–260.

Cromie, P.W., Gosse, R.R., Zhang, P., Zhu, X., 1996. Exploration for carbonate-hosted Pb–Zn deposits, Sichuan, P.R.C. [abs.]. International Geological Congress, 30th, Beijing, China, p. 412 (Abstracts).
Czamanske, G.K., Rye, R.O., 1974. Experimentally determined sulfur isotope fractionations between sphalerite and galena in the temperature range 600 °C to 275 °C. Econ. Geol. 69, 17–25.
Demény, A., Harangi, S.Z., 1996. Stable isotope studies on carbonate formations in alkaline basalt and lamprophyre series: evolution of magmatic fluids and magma–sediment interactions. Lithos 37, 335–349.
Demény, A., Ahijado, A., Casillas, R., Vennemann, T.W., 1998. Crustal contamination and fluid/rock interaction in the carbonatites of Fuerteventura (Canary Islands, Spain): a C, O, H isotope study. Lithos 44, 101–115.
Deng, H.L., Li, C.Y., Tu, G.Z., Zhou, Y.M., Wang, C.W., 2000. Strontium isotope geochemistry of the Lemachang independent silver ore deposit, northeastern Yunnan, China. Sci. China Ser. D Earth Sci. 43, 337–346.
Dixon, G., Davidson, G.J., 1996. Stable isotope evidence for thermo chemical sulfate reduction in the Dugald River (Australia) strata-bound shale-hosted zinc–lead deposit. Chem. Geol. 129, 227–246.
Faure, G., 1977. Principles of Isotope Geology. John Wiley & Sons, New York pp. 28–110.
Fontbote, L., Gorzawski, H., 1990. Genesis of the Mississippi Valley-type Zn–Pb deposit of San Vicente, central Peru: geologic and isotopic (Sr, O, C, S, Pb) evidence. Econ. Geol. 85, 1402–1437.
Fu, S.H., 2004. Metallogenesis of Pb–Zn Deposits and Enrichment Regularity of Dispersed Elements Cd, Ga and Ge in SW Yangtze Block. Ph.D. Thesis , Chengdu University of Science and Technology, Chengdu, China pp. 20–67 (in Chinese with English abstract).
Fujii, T., Moynier, F., Pons, M.L., Albarède, F., 2011. The origin of Zn isotope fractionation in sulfides. Geochim. Cosmochim. Acta 75, 7632–7643.
Gagnevin, D., Boyce, A.J., Barrie, C.D., Menuge, J.F., Blakeman, R.J., 2012. Zn, Fe and S isotope fractionation in a large hydrothermal system. Geochim. Cosmochim. Acta 88, 183–198.
Gao, S., Yang, J., Zhou, L., Li, M., Hu, Z., Guo, J., Yuan, H., Gong, H., Xiao, G., Wei, J., 2011. Age and growth of the Archean Kongling terrain, South China, with emphasis on 3.3 Ga granitoid gneisses. Am. J. Sci. 311, 153–182.
Gray, D.R., Gregory, R.T., Durney, D.W., 1991. Rock-buffered fluid–rock interaction in deformed quartz-rich turbidite sequences, eastern Australia. J. Geophys. Res. Solid Earth 96, 19681–19704.
Gromek, P., Gleeson, S.A., Simonetti, A., 2012. A basement-interacted fluid in the N81 deposit, Pine Point Pb–Zn district, Canada: Sr isotopic analyses of single dolomite crystals. Miner. Deposita 47, 749–754.
Haest, M., Schneider, J., Cloquet, C., Latruwe, K., Vanhaecke, F., Muchez, P., 2010. Pb isotopic constraints on the formation of the Dikulushi Cu–Pb–Zn–Ag mineralisation, Kundelungu Plateau (Democratic Republic of Congo). Miner. Deposita 45, 393–410.
Han, R.S., Liu, C.Q., Huang, Z.L., Chen, J., Ma, D.Y., Lei, L., Ma, G.S., 2007a. Geological features and origin of the Huize carbonate-hosted Zn–Pb–(Ag) district, Yunnan, South China. Ore Geol. Rev. 31, 360–383.
Han, R.S., Zou, H.J., Hu, B., Hu, Y.Z., Xue, C.D., 2007b. Features of fluid inclusions and sources of ore-forming fluid in the Maoping carbonate-hosted Zn–Pb–(Ag–Ge) deposit, Yunnan, China. Acta Petrol. Sin. 23, 2109–2118.
Heijlen, W., Muchez, P., Banks, D.A., Schneider, J., Kucha, H., Keppens, E., 2003. Carbonate-hosted Zn–Pb deposits in Upper Silesia, Poland: origin and evolution of mineralizing fluids and constraints on genetic models. Econ. Geol. 98, 911–932.
Hu, Y.G., 1999. Ag Occurrence, Source of Ore-Forming Metals and Mechanism of Yinchangpo Ag–Pb–Zn Deposit, Guizhou. Ph.D. Thesis , Institute of Geochemistry, Chinese Academy of Sciences pp. 10–55 (in Chinese with English abstract).
Hu, R.Z., Zhou, M.F., 2012. Multiple Mesozoic mineralization events in South China—an introduction to the thematic issue. Miner. Deposita 47, 579–588.
Huang, Z.L., Li, W.B., Chen, J., Han, R.S., Liu, C.Q., Xu, C., Guan, T., 2003. Carbon and oxygen isotope constraints on the mantle fluids join the mineralization of the Huize super-large Pb–Zn deposits, Yunnan Province, China. J. Geochem. Explor. 78/79, 637–642.
Huang, Z.L., Chen, J., Han, R.S., Li, W.B., Liu, C.Q., Zhang, Z.L., Ma, D.Y., Gao, D.R., Yang, H.L., 2004. Geochemistry and ore-formation of the Huize giant lead–zinc deposit, Yunnan, Province, China. Discussion on the Relationship Between Emeishan Flood Basalts and Lead–Zinc Mineralization. Geological Publishing House, Beijing, pp. 1–204 (in Chinese).
Huang, Z.L., Li, X.B., Zhou, M.F., Li, W.B., Jin, Z.G., 2010. REE and C–O isotopic geochemistry of calcites from the world-class Huize Pb–Zn deposit, Yunnan, China: implications for the ore genesis. Acta Geol. Sin. (Engl. Ed.) 84, 597–613.
Jian, P., Li, D.Y., Kröner, A., Zhang, Q., Wang, Y.Z., Sun, X.M., Zhang, W., 2009. Devonian to Permian plate tectonic cycle of the Paleo-Tethys Orogen in southwest China (II): insights from zircon ages of ophiolites, arc/back-arc assemblages and within-plate igneous rocks and generation of the Emeishan CFB province. Lithos 113, 767–784.
Jin, Z.G., 2008. The ore-Control Factors, Ore-Forming Regularity and Forecasting of Pb–Zn Deposit, in Northwestern Guizhou Province. Engine Industry Press, Beijing pp. 1–105 (in Chinese).
John, S.G., Rouxel, O.J., Craddock, P.R., Engwall, A.M., Boyle, E.A., 2008. Zinc stable isotopes in seafloor hydrothermal vent fluids and chimneys. Earth Planet. Sci. Lett. 269, 17–28.
Jorgenson, B.B., Isaksen, M.F., Jannasch, H.W., 1992. Bacterial sulfate reduction above 100 °C in deep sea hydrothermal vent sediments. Science 258, 1756–1757.
Kelley, K.D., Wilkinson, J.J., Chapman, J.B., Crowther, H.L., Weiss, D.J., 2009. Zinc isotopes in sphalerite from base metal deposits on the Red Dog district, Northern Alaska. Econ. Geol. 104, 767–773.
Leach, D.L., Bradley, D., Lewchuk, M.T., Symons, D.T.A., de Marsily, G., Brannon, J., 2001. Mississippi Valley type lead–zinc deposits through geological time: implications from recent age-dating research. Miner. Deposita 36, 711–740.
Leach, D.L., Sangster, D., Kelley, K., Large, R.R., Garven, G., Allen, C., Gutzmer, J., Walters, S.G., 2005. Sediment-Hosted Lead–Zinc Deposits: A Global Perspective. Economic Geology 100th Anniversary Volume, pp. 561–608.
Leach, D.L., Bradley, D.C., Huston, D., Pisarevsky, S.A., Taylor, R.D., Gardoll, S.J., 2010. Sediment-hosted lead–zinc deposits in Earth history. Econ. Geol. 105, 593–625.
Li, F.H., Qin, J.M., 1988. Presinian System in Kangdian Area. Chongqing Press, Chongqing pp. 15–45 (in Chinese).
Li, Q.L., Chen, F.K., Wang, X.L., Li, C.F., 2005. Ultra-low procedural blank and the single grain mica Rb–Sr isochron dating. Chin. Sci. Bull. 50, 2861–2865.
Li, W.B., Huang, Z.L., Yin, M.D., 2007a. Isotope geochemistry of the Huize Zn–Pb ore field, Yunnan province, southwestern China: implication for the sources of ore fluid and metals. Geochem. J. 41, 65–81.
Li, W.B., Huang, Z.L., Yin, M.D., 2007b. Dating of the giant Huize Zn–Pb ore field of Yunnan province, southwest China: constraints from the Sm–Nd system in hydrothermal calcite. Resour. Geol. 57, 90–97.
Li, S.Z., Zhu, X.K., Tang, S.H., He, X.X., Cai, J.J., 2008. The application of MC-ICP-MS to high-precision measurement of Zn isotope ratios. Acta Petrol. Mineral. 27, 273–278 (in Chinese with English abstract).
Lin, Z.Y., Wang, D.H., Zhang, C.Q., 2010. Rb–Sr isotopic age of sphalerite from the Paoma lead–zinc deposit in Sichuan Province and its implications. Geol. China 37 (488–196), (in Chinese with English abstract).
Liu, H.C., Lin, W.D., 1999. Study on the Law of Pb–Zn–Ag Ore Deposit in Northeast Yunnan, China. Yunnan University Press, Kunming pp. 1–468 (in Chinese).
Liu, J.M., Liu, J.J., 1997. Basin fluid genetic model of sediment-hosted micro-disseminated gold deposits in the gold-triangle area between Guizhou, Guangxi and Yunnan. Acta Miner. Sin. 17, 448–456 (in Chinese with English abstract).
Machel, H.G., Krouse, H.R., Sassen, R., 1995. Products and distinguishing criteria of bacterial and thermo-chemical sulfate reduction. Appl. Geochem. 10, 373–389.
Mao, J.Q., Zhang, Q.H., Gu, S.Y., 1998. Tectonic Evolution and Pb–Zn Mineralization of Shuicheng Fault Subsidence. Guizhou Science and Technology Publishing Company, Guiyang pp. 104–129 (in Chinese).
Mao, J.W., Zhou, Z.H., Feng, C.Y., Wang, Y.T., Zhang, C.Q., Peng, H.J., Miao, Y., 2012. A preliminary study of the Triassic large-scale mineralization in China and its geodynamic setting. Geol. China 39, 1437–1471 (in Chinese with English abstract).
Maréchal, C.N., Sheppard, S.M.F., 2002. Isotopic fractionation of Cu and Zn between chloride and nitrate solutions and malachite or smithsonite at 30 °C and 50 °C. Goldschmidt Conference. Geochim. Cosmochim. Acta 66, A484.
Maréchal, C.N., Télouk, P., Albarède, F., 1999. Precise analysis of copper and zinc isotopic compositions by plasma-source mass spectrometry. Chem. Geol. 156, 251–273.
Mason, T.F.D., Weiss, D.J., Horstwood, M., Parrish, R.R., Russell, S.S., Mullance, E., Coles, J.B., 2004a. High-precision Cu and Zn isotope analysis by plasma source mass spectrometry: part 1 spectral interferences and their correction. J. Anal. At. Spectrom. 19, 209–217.
Mason, T.F.D., Weiss, D.J., Horstwood, M., Parrish, R.R., Russell, S.S., Mullance, E., Coles, J.B., 2004b. High-precision Cu and Zn isotope analysis by plasma source mass spectrometry: part 2 correction for mass discrimination effects. J. Anal. Atom. Spectrom. 19, 218–226.
Mason, T.F.D., Weiss, D.J., Chapman, J.B., Wilkinson, J.J., Tessalina, S.G., Spiro, B., Horstwood, M.S.A., Spratt, J., Coles, B.J., 2005. Zn and Cu isotopic variability in the Alexandrinka volcanic-hosted massive sulphide (VHMS) ore deposit, Urals, Russia. Chem. Geol. 221, 170–187.
Mirnejad, H., Simonetti, A., Molasalehi, F., 2011. Pb isotopic compositions of some Zn–Pb deposits and occurrences from Urumieh–Dokhtar and Sanandaj–Sirjan Zones in Iran. Ore Geol. Rev. 39, 181–187.
Muchez, P., Slobodník, M., Viaene, W.A., Keppens, E., 1995. Geochemical constraints on the origin and migration of palaeofluids at the northern margin of the Variscan foreland, southern Belgium. Sediment. Geol. 96, 191–200.
Muchez, P., Heijlen, W., Banks, D., Blundell, D., Boni, M., Grandia, F., 2005. Extensional tectonics and the timing and formation of basin-hosted deposits in Europe. Ore Geol. Rev. 27, 241–267.
Ohmoto, H., Goldhaber, M.B., 1997. Sulfur and carbon isotopes, In: Barnes, H.L. (Ed.), Geochemistry of Hydrothermal Ore Deposits, 3rd ed. Wiley and Sons, New York, pp. 517–611.
Ohmoto, H., Rye, R.O., 1979. Isotopes of sulfur and carbon, In: Barnes, H.L. (Ed.), Geochemistry of Hydrothermal Ore Deposits, 2nd ed. Wiley and Sons, New York, pp. 509–567.
Ohmoto, H., Kaiser, C.J., Geer, K.A., 1990. Systematics of Sulphur Isotopes in Recent Marine Sediments and Ancient Sediment-Hosted Base Metal Deposits. In: Herbert, H.K., Ho, S. E. (Eds.), Stable isotopes and Fluid Processes in Mineralisation. 23. Geol. Dep. Univ. Extens. Univ, Western Australia, pp. 70–120.
Oliver, J., 1986. Fluids expelled tectonically from orogenic belts: their role in hydrocarbon migration and other geologic phenomena. Geology 14, 99–102.
Oliver, J., 1992. The spots and stains of plate tectonics. Earth Sci. Rev. 32, 77–106.
Pinckney, D.M., Rafter, T.A., 1972. Fractionation of sulfur isotopes during ore deposition in the Upper Mississippi Valley zinc–lead district. Econ. Geol. 67, 315–328.
Pirajno, F., 2009. Hydrothermal Processes and Mineral Systems. Springer, Berlin p. 1256.
Pirajno, F., 2013. The Geology and Tectonic Setting of China's Mineral Deposits. Springer, Berlin pp. 123–183.
Powell, T.G., Macqueen, R.W., 1984. Precipitation of sulfide ores and organic matter: sulfate reactions at Pine Point, Canada. Science 224, 63–66.
Qiu, Y.M., Gao, S., McNaughton, N.J., Groves, D.I., Ling, W.L., 2000. First evidence of >3.2 Ga continental crust in the Yangtze craton of south China and its implications for Archean crustal evolution and Phanerozoic tectonics. Geology 28, 11–14.
Reid, A., Wilson, C.J.L., Shun, L., Pearson, N., Belousova, E., 2007. Mesozoic plutons of the Yidun Arc, SW China: U/Pb geochronology and Hf isotopic signature. Ore Geol. Rev. 31, 88–106.
Seal, I.R., 2006. Sulfur isotope geochemistry of sulfide minerals. Rev. Mineral. Geochem. 61, 633–677.
Sun, W.H., Zhou, M.F., Gao, G.F., Yang, Y.H., Zhao, X.F., Zhao, J.H., 2009. Detrital zircon U–Pb geochronological and Lu–Hf isotopic constraints on the Precambrian magmatic and crustal evolution of the western Yangtze Block, SW China. Precambrian Res. 172, 99–126.

Sverjensky, D.A., 1981. The origin of a Mississippi valley-type deposit in the Viburnum Trend, south Missouri. Econ. Geol. 76, 1848–1872.
Tang, S.H., Zhu, X.K., Cai, J.J., Li, S.Z., He, X.X., Wang, J.H., 2006. Chromatographic separation of Cu, Fe and Zn using AG M P-1 anion exchange resin for isotope determination by MC-ICPMS. Rock Mineral Anal. 25, 5–8 (in Chinese with English abstract).
Taylor, J.H.P., Frechen, J., Degens, E.T., 1967. Oxygen and carbon isotope studies of carbonatites from the Laacher See District, West Germany and the Alno District Sweden. Geochim. Cosmochim. Acta 31, 407–430.
Toutain, J.P., Sonke, J., Munoz, M., Nonell, A., Polvé, M., Viers, J., Freydier, R., Sortino, F., Joron, J.L., Sumarti, S., 2008. Evidence for Zn isotopic fractionation at Merapi volcano. Chem. Geol. 253, 74–82.
Veizer, J., Hoefs, J., 1976. The nature of $^{18}O/^{16}O$ and $^{13}C/^{12}C$ secular trends in sedimentary carbonate rocks. Geochim. Cosmochim. Acta 40, 1387–1395.
Wang, X.C., Zheng, Z.R., Zheng, M.H., Xu, X.H., 2000. Metallogenic mechanism of the Tianbaoshan Pb–Zn deposit, Sichuan. Chin. J. Geochem. 19, 121–133.
Wang, J.Z., Li, Z.Q., Ni, S.J., 2003. Origin of ore-forming fluids of Mississippi Valley-type (MVT) Pb–Zn deposits in Kangdian area, China. Chin. J. Geochem. 22, 369–376.
Wang, W., Wang, F., Chen, F.K., Zhu, X.Y., Xiao, P., Siebel, W., 2010. Detrital zircon ages and Hf–Nd isotopic composition of Neoproterozoic sedimentary rocks in the Yangtze Block: constraints on the deposition age and provenance. J. Geol. 118, 79–94.
Wang, W., Zhou, M.F., Yan, D.P., Li, J.W., 2012. Depositional age, provenance, and tectonic setting of the Neoproterozoic Sibao Group, southeastern Yangtze Block, South China. Precambrian Res. 192–195, 107–124.
Wilkinson, J.J., Weiss, D.J., Mason, T.F.D., Coles, B.J., 2005. Zinc isotope variation in hydrothermal systems: preliminary evidence from the Irish Midlands ore field. Econ. Geol. 100, 583–590.
Xie, J.R., 1963. Introduction of the Chinese Ore Deposits. Scientific books Publishing House, Beijing pp. 1–71 (in Chinese).
Yan, D.P., Zhou, M.F., Song, H.L., Wang, X.W., Malpas, J., 2003. Origin and tectonic significance of a Mesozoic multi-layer over-thrust system within the Yangtze Block (South China). Tectonophysics 361, 239–254.
Ye, L., Cook, N.J., Ciobanu, C.L., Liu, Y.P., Zhang, Q., Liu, T.G., Gao, W., Yang, Y.L., Danyushevsky, L., 2011. Trace and minor elements in sphalerite from base metal deposits in South China: a LA-ICPMS study. Ore Geol. Rev. 39, 188–217.
Zartman, R.E., Doe, B.R., 1981. Plumbotectonics—the model. Tectonophysics 75, 135–162.
Zaw, K., Peters, S.G., Cromie, P., Burrett, C., Hou, Z., 2007. Nature, diversity of deposit types and metallogenic relations of South China. Ore Geol. Rev. 31, 3–47.
Zhang, Q.H., Mao, J.Q., Guang, S.Y., 1998. The studies of ore-forming material sources of metal deposit in Hezhang Pb–Zn mine Shuicheng, Guizhou province. J. Guizhou Univ. Technol. 27, 26–34 (in Chinese with English abstract).
Zhang, Q., Liu, J.J., Shao, S.X., 2002. An estimate of the lead isotopic compositions of upper mantle and upper crust and implications for the source of lead in the Jinding Pb–Zn deposit in western Yunnan, China. Geochem. J. 36, 271–287.
Zhao, X.F., Zhou, M.F., Li, J.W., Sun, M., Gao, J.F., Sun, W.H., Yang, J.H., 2010. Late Paleoproterozoic to early Mesoproterozoic Dongchuan Group in Yunnan, SW China: implications for tectonic evolution of the Yangtze Block. Precambrian Res. 182, 57–69.
Zheng, C.L., 1994. An approach on the sources of ore-forming metals for lead–zinc deposits in northwest Guizhou province. J. Guilin Coll. Geol. 14, 113–124 (in Chinese with English abstract).
Zheng, M.H., Wang, X.C., 1991. Genesis of the Daliangzi Pb–Zn deposit in Sichuan, China. Econ. Geol. 86, 831–846.
Zhou, C.X., Wei, C.S., Guo, J.Y., 2001. The source of metals in the Qilingchang Pb–Zn deposit, Northeastern Yunnan, China: Pb–Sr isotope constraints. Econ. Geol. 96, 583–598.
Zhou, M.F., Malpas, J., Song, X.Y., Robinson, P.T., Sun, M., Kennedy, A.K., Lesher, C.M., Keays, R.R., 2002. A temporal link between the Emeishan large igneous province (SW China) and the end-Guadalupian mass extinction Earth. Earth Planet. Sci. Lett. 196, 113–122.
Zhou, J.X., Huang, Z.L., Zhou, G.F., Li, X.B., Ding, W., Bao, G.P., 2011. Trace elements and rare earth elements of sulfide minerals in the Tianqiao Pb–Zn ore deposit, Guizhou province, China. Acta Geol. Sin. (Engl. Ed.) 85, 189–199.
Zhou, J.X., Huang, Z.L., Zhou, M.F., Li, X.B., Jin, Z.G., 2013a. Constraints of C–O–S–Pb isotope compositions and Rb–Sr isotopic age on the origin of the Tianqiao carbonate-hosted Pb–Zn deposit, SW China. Ore Geol. Rev. 53, 77–92.
Zhou, J.X., Huang, Z.L., Bao, G.P., 2013b. Geological and sulfur–lead–strontium isotopic studies of the Shaojiwan Pb–Zn deposit, southwest China: implications for the origin of hydrothermal fluids. J. Geochem. Explor. 128, 51–61.
Zhou, J.X., Huang, Z.L., Gao, J.G., Yan, Z.F., 2013c. Geological and C–O–S–Pb–Sr isotopic constraints on the origin of the Qingshan carbonate-hosted Pb–Zn deposit, SW China. Int. Geol. Rev. 55, 904–916.
Zhou, J.X., Huang, Z.L., Yan, Z.F., 2013d. The origin of the Maozu carbonate-hosted Pb–Zn deposit, southwest China: constrained by C–O–S–Pb isotopic compositions and Sm–Nd isotopic age. J. Asian Earth Sci. 73, 39–47.
Zhou, J.X., Gao, J.G., Chen, D., Liu, X.K., 2013e. Ore genesis of the Tianbaoshan carbonate-hosted Pb–Zn deposit, Southwest China: geologic and isotopic (C–H–O–S–Pb) evidence. Int. Geol. Rev. 55, 1300–1310.
Zhou, J.X., Huang, Z.L., Zhou, M.F., Zhu, X.K., Muchez, P., 2014. Zinc, sulfur and lead isotopic variations in carbonate-hosted Pb–Zn sulfide deposits, southwest China. Ore Geol. Rev. 58, 41–54.
Zhu, X.K., O'Nions, R.K., Guo, Y., Belshaw, N.S., Rickard, D., 2000. Determination of natural Cu isotope variation by plasmas source mass spectrometry: implications for use as geochemical tracers. Chem. Geol. 163, 139–149.
Zhu, X.K., Guo, Y., Williams, R.J.P., O'Nions, R.K., Matthews, A., Belshaw, N.S., Canters, G.W., Waal, E.C.D., Weser, U., Burgess, B.K., Salvato, B., 2002. Mass fractionation processes of transition metal isotopes. Earth Planet. Sci. Lett. 200, 47–62.